Atmospheric
Chemistry
and Physics

The contribution of plume-scale nucleation to global and regional aerosol and CCN concentrations: evaluation and sensitivity to emissions changes

R. G. Stevens[1,2] **and J. R. Pierce**[1,2]

[1]Department of Physics and Atmospheric Science, Dalhousie University, Halifax, NS, Canada
[2]Department of Atmospheric Science, Colorado State University, Fort Collins, CO, USA

Correspondence to: R. G. Stevens (rgsteven@dal.ca)

Abstract. We implement the Predicting Particles Produced in Power-Plant Plumes (P6) sub-grid sulphate parameterization for the first time into a global chemical-transport model with online aerosol microphysics, the GEOS-Chem-TOMAS model. Compared to simulations using two other previous treatments of sub-grid sulphate, simulations using P6 sub-grid sulphate predicted similar or smaller increases (depending on other model assumptions) in globally, annually averaged concentrations of particles larger than 80 nm (N80). We test in simulations using P6 sub-grid sulphate the sensitivity of particle number concentrations to changes in SO_2 or NO_x emissions to represent recent emissions control changes. For global increases of 50 % in emissions of either SO_2 or NO_x, or both SO_2 and NO_x, we find that globally, annually averaged N80 increase by 9.00, 1.47, or 10.24 % respectively. However, both sub-grid and grid-resolved processes contribute to these changes. Finally, we compare the model results against observations of particle number concentrations. Compared with previous treatments of sub-grid sulphate, use of the P6 parameterization generally improves correlation with observed particle number concentrations. The P6 parameterization is able to resolve spatial heterogeneity in new-particle formation and growth that cannot be resolved by any constant assumptions about sub-grid sulphate. However, the differences in annually averaged aerosol size distributions due to the treatment of sub-grid sulphate at the measurement sites examined here are too small to unambiguously establish P6 as providing better agreement with observations.

1 Introduction

Anthropogenic aerosol affects human health and the Earth's climate. High aerosol concentrations cause human health problems, including respiratory and cardiovascular diseases, intensification of asthma, a reduction in physical abilities and an increase in mortality rates (Arya, 1999; Dockery et al., 1993; Peng et al., 2005; Stieb et al., 2002). Particles smaller than 100 nm in diameter may have greater health impacts than larger particles (Peters et al., 1997). Aerosols also affect the Earth's climate through direct radiative effects (Charlson et al., 1992) and through indirect radiative effects: changes in cloud reflectivity and lifetime due to changes in the number of aerosol particles acting as Cloud Condensation Nuclei (CCN) (Albrecht, 1989; Twomey, 1974). Both of these aerosol effects are strongly dependent on the size of the aerosol and the magnitude of these effects have large uncertainties (Boucher et al., 2013; Dusek et al., 2006).

One of the largest anthropogenic sources of aerosol mass are sulphur-rich plumes (Dentener et al., 2006). The hydroxyl radical (OH) can oxidize sulphur dioxide (SO_2) within these plumes to form sulphuric acid (H_2SO_4), which in turn can condense onto pre-existing particles. If H_2SO_4 concentrations are high enough, the H_2SO_4 will cluster with itself and other condensible gases to nucleate new particles (Kulmala and Kerminen, 2008). Anthropogenic sulphur emissions have been shown to have a significant effect on global particle concentrations, particularly in the Northern Hemisphere (Adams and Seinfeld, 2003; Luo and Yu, 2011; Spracklen et al., 2005; Wang and Penner, 2009); however,

the magnitude of this impact depends on assumptions made in the modelling studies as will be discussed.

There are several factors that determine the rate of particle formation and growth in the plumes of coal-fired power plants. These include the solar radiation and NO_x concentrations (through their influence on OH concentrations), and the pre-existing condensation and coagulation sinks. Further complicating the formation and growth rates are that many of these factors vary spatially in the plume. Concentrations of OH in the plume control the SO_2 gas-phase oxidation rate and hence influence H_2SO_4 concentrations. These OH concentrations depend strongly on NO_x (nitric oxide (NO) + nitrogen dioxide (NO_2)) concentrations and sunlight (Olson et al., 2006). The primary loss mechanism for H_2SO_4 in the boundary layer is condensation onto existing aerosol particles (Eisele and Tanner, 1993), and so concentrations of H_2SO_4 also depend strongly on the aerosol condensation sink (approximately proportional to aerosol surface area). The variation in NO_x concentrations and the heterogeneity of the condensation sink within a given plume causes H_2SO_4 concentrations to vary dramatically within the plume (Stevens et al., 2012; Lonsdale et al., 2012). Nucleation and growth rates are strong functions of H_2SO_4 concentrations, and will therefore vary spatially across the plume. Finally, the newly formed particles may be lost by coagulation with larger particles; as the size distribution evolves spatially in the plume, so will these coagulational losses. Currently, the resolutions of regional- and global-scale models are typically at least tens or hundreds of kilometres, respectively. These models are therefore unable to accurately resolve the formation and growth of aerosols within these plumes using grid-box averages for chemical concentrations, aerosol concentrations, and meteorological values.

These models have therefore typically assumed that some fraction of all anthropogenic SO_2 emissions are oxidized to form sulphate (SO_4) at the sub-grid scale. This sub-grid sulphate is added to the model via a fixed, pre-assumed size distribution for all anthropogenic sulphate sources. For instance, the study of Makkonen et al. (2009) used the assumption recommended by the AeroCom emissions inventory (Dentener et al., 2006): they emitted the sulphate into a single lognormal mode with a median radius of 500 nm and a standard deviation of 2.0. Many studies (Adams and Seinfeld, 2002, 2003; Pierce and Adams, 2006, 2009; Pierce et al., 2007; Spracklen et al., 2005; Wang and Penner, 2009) have used a bi-modal distribution comprised of a nucleation mode and an Aitken mode with number median diameters 10 nm and 70 nm, and geometric standard deviations 1.6 and 2.0. Either 5 or 15 % of the sulphate mass is emitted into the nucleation mode, depending on the study. Several of these studies investigated the sensitivity to the assumptions made about sub-grid sulphate formation. Adams and Seinfeld (2003) and Spracklen et al. (2005) found that if they changed the fraction of SO_2 converted to sub-grid sulphate from 0 to 3 %, CCN at an assumed supersaturation of 0.2 % (CCN(0.2 %))

in polluted areas would double. Both models included only sulphate and sea-salt aerosol, so this was believed to be an upper limit for this effect. But the study of Wang and Penner (2009), which included organic matter, black carbon, and dust, varied the fraction of SO_2 converted to sub-grid sulphate over a smaller range (between 0 and 2 %), and also found that CCN(0.2 %) more than doubled over polluted areas. Additionally, they found that CCN(0.2 %) increased by either 23 or 53 % averaged over the global boundary layer, and that the aerosol indirect effect radiative forcing increased by either 11 or 31 % (depending on the grid-resolved nucleation scheme used in the boundary layer). The study of Yu and Luo (2009) used yet another approach for representing sub-grid sulphate: of the emitted SO_2 assumed to form sulphate on the sub-grid scale, 5 % of sulphur mass is emitted directly into the nucleation mode described above and the remaining mass is condensed onto the existing accumulation-mode particles. As some of the sulphate formed in the plume must condense onto the pre-existing particles that have been entrained into the plume, this approach is, in this way, more realistic than the other assumptions. Luo and Yu (2011) varied the fraction of sulphate emitted into the nucleation mode from 5 to 15 %, and found that CCN(0.2 %) increased by up to 18 % over source regions. Furthermore, they found that changing the fraction of emitted SO_2 converted to sub-grid sulphate from 0 to 5 % changed global boundary-layer CCN(0.2 %) by 11 %. Hence, CCN concentrations and regional radiative forcings are clearly sensitive to the assumptions regarding sulphur partitioning and the size of aerosol formed in sulphur-rich plumes.

Lee et al. (2013) recently quantified the uncertainty in CCN concentrations that was due to 28 different parameters in the GLOMAP global aerosol model. They found that the uncertainties in sub-grid sulphate production contributed just as much to uncertainties in CCN concentrations as those of SO_2 emission, and had the largest contribution of the 28 inputs to the uncertainty in CCN concentrations over polluted North America and Europe. The global uncertainty in sub-grid sulphate particle size ranked as the twelfth largest contributor to the relative uncertainties in CCN concentrations of the 28 inputs tested. Based on the results of Stevens et al. (2012), the range of possible values for the diameter of sub-grid-sulphate particles used in Lee et al. (2013) was reduced to a smaller range than the full range of sub-grid-sulphate assumptions used in the studies cited in the preceding paragraphs. This reduced range would lead to a reduced uncertainty range in CCN concentrations as described in the previous paragraph. These large uncertainties in CCN prediction due to sub-grid sulphate formation highlight the need for improved representation of plume-scale particle formation in global and regional models.

In order to more accurately represent this sub-grid sulphate, Stevens and Pierce (2013) introduced a parameterization that predicts the characteristics of aerosol formed in point-source plumes based on variables commonly available

in global- and regional-scale models. Specifically, the Predicting Particles Produced in Power-Plant Plumes (P6) parameterization predicts the fraction of SO_2 oxidized to form H_2SO_4 (f_{ox}), the fraction of the H_2SO_4 that forms new particles (f_{new}), the number of new particles formed per kg SO_2 emitted (N_{new}), and the median diameter of the newly formed particles (D_m). The P6 parameterization takes as inputs the emissions of SO_2 (E_{SO_2}) and NO_x (E_{NO_x}) from the power-plant, the pre-existing aerosol condensation sink (CS), the downward shortwave radiative flux (DSWRF), the mean boundary-layer wind speed (v_g), the boundary-layer height (BLH), the distance from the source (d), and the background concentrations of SO_2 (bgSO_2) and NO_x (bgNO_x). In this paper, we implement this parameterization into a global aerosol microphysics model to estimate the contribution of sub-grid-sulphate formation to aerosol size distributions and CCN.

Additionally, recent pollution-control technologies installed on power plants reduce SO_2 and NO_x emissions. A reduction in SO_2 alone would result in a reduction of particles formed in power-plant plumes. However, concentrations of OH are sensitive to NO_x concentrations, which will vary across a given plume (Lonsdale et al., 2012). NO_x controls may either increase or decrease OH concentrations in the plume (depending on the environmental conditions). Hence, in many conditions reducing NO_x concentrations may increase the formation rate of H_2SO_4 and increase particle formation and growth. The P6 parameterization has been designed to reproduce these effects of changes in SO_2 and NO_x emissions on particle formation and growth. Use of some pollution-control technologies, such as selective catalytic reduction and flue gas desulphurisation, may result in formation of sulphur trioxide within the emissions stack, which would quickly form H_2SO_4 and could result in new-particle formation within the emissions stack (Junkermann et al., 2011; Srivastava et al., 2004). However, these effects are not yet resolved by P6 and so will not be discussed in this work.

In this paper, we implement the P6 sub-grid sulphate parameterization (Stevens and Pierce, 2013) into a global chemical-transport model with online aerosol microphysics. We test the sensitivities of predicted N3, N10, N40, N80 (the number concentration of particles with diameters larger than 3, 10, 40 and 80 nm, respectively) to assumptions about sub-grid sulphate. As the output of the P6 parameterization is expected to be sensitive to pre-existing aerosol via condensation and coagulation sinks, we investigate the sensitivity of predictions to the global amount of secondary organic aerosol and grid-resolved nucleation scheme. In order to better understand the effects of pollution controls on CCN concentrations, we also investigate the sensitivity of the N80 enhancement from sub-grid sulphate to greater emissions of SO_2 and NO_x.

In Sect. 2, we describe the GEOS-Chem-TOMAS model specifications and we describe the simulations performed for this study. In Sect. 3 we discuss the sensitivities of our results

to the treatment of sub-grid sulphate, and how these interact with additional secondary organic aerosol emissions and grid-resolved nucleation scheme. In Sect. 4 we present the results of the P6 Gradient Subroutine, and discuss the sensitivity of our results to the inputs of P6. In Sect. 5 we discuss the sensitivities to SO_2 and NO_x emissions. In Sect. 6 we compare the results of our simulations with surface-based N10, N40, N80, and N150 measurements. Finally, we present our conclusions in Sect. 7.

## 2 Model specifications and descriptions of simulations

For this study, we implemented the P6 sub-grid sulphate parameterization into the GEOS-Chem-TOMAS model. GEOS-Chem-TOMAS uses the TwO Moment Aerosol Sectional (TOMAS) microphysics algorithm (Adams and Seinfeld, 2002; Pierce and Adams, 2009) in the GEOS-Chem v9-02 chemical transport model (http://geos-chem.org, Bey et al., 2001). The implementation of TOMAS in GEOS-Chem has been discussed previously (Pierce et al., 2013; Snow-Kropla et al., 2011; Trivitayanurak et al., 2008). The TOMAS module resolves aerosol by both mass and number independently. For this study, the aerosol was simulated using 15 size bins spanning 3 nm to 10 µm (Lee and Adams, 2012). Condensation, coagulation, and nucleation are explicitly resolved in the model. The model was run at 4° latitude by 5° longitude resolution with 47 vertical layers from the surface to 0.01 hPa and with meteorological inputs from the GEOS5 re-analysis (http://gmao.gsfc.nasa.gov).

Anthropogenic emissions in GEOS-Chem are provided by the Emissions Database for Global Atmospheric Research (EDGAR) inventory (Olivier et al., 1996), except where it is overwritten by the following regional inventories: The Environmental Protection Agency 2005 National Emissions Inventory (NEI05) (http://www.epa.gov/ttn/chief/net/2005inventory.html) over the United States, the Criteria Air Contaminants (CAC) for anthropogenic emissions over Canada (http://www.ec.gc.ca/inrp-npri/), the Big Bend Regional Aerosol and Visibility Study (BRAVO) emissions inventory over Mexico and the southwestern United States (Kuhns et al., 2001), the Streets inventory for Asian emissions (Streets et al., 2003) over Asia, and the Cooperative Programme for Monitoring and Evaluation of the Long-Range Transmission of Air Pollutants in Europe (EMEP) over Europe (Auvray and Bey, 2005). The total annual fossil-fuel SO_2 emissions, not including shipping emissions, from these inventories are shown in Fig. 1 for the simulated year, 2005. Biogenic emissions were from the Model of Emissions of Gases and Aerosols from Nature (MEGAN) (Guenther et al., 2006), except for an additional secondary organic aerosol (SOA) source in some simulations that we will describe below. Biomass burning emissions were from the Global Fire Emissions Database version 3 (GFEDv3) (van der Werf et al., 2010).

The P6 parameterization predicts characteristics of sub-grid sulphate formed in sulphur-rich plumes based on variables commonly available in global- and regional-scale models. A full description is available in Stevens and Pierce (2013). Specifically, the parameterization predicts the fraction of SO_2 oxidized to form H_2SO_4 (f_{ox}), the fraction of the H_2SO_4 that forms new particles (f_{new}), the number of new particles formed per kg SO_2 emitted (N_{new}), and the median diameter of the newly formed particles (D_m). The parameterization takes as inputs the emissions of SO_2 (E_{SO_2}) and NO_x (E_{NO_x}) from the power-plant, the pre-existing aerosol condensation sink (CS), the downward shortwave radiative flux (DSWRF), the mean boundary-layer wind speed (v_g), the boundary-layer height (BLH), the distance from the source (d), and the background concentrations of SO_2 ($bgSO_2$) and NO_x ($bgNO_x$).

The P6 parameterization is based upon the results of the System for Atmospheric Modelling (SAM) (Khairoutdinov and Randall, 2003) with the TOMAS microphysics module described above. The SAM-TOMAS model is a complex Large-Eddy Simulation/Cloud Resolving Model capable of resolutions between tens of metres and hundreds of kilometres and domains between tens and hundreds of kilometres. The P6 parameterization therefore inherits some limitations of SAM-TOMAS model. It does not account for new-particle formation due to possible direct emissions of sulphur trioxide (SO_3) or nitrous acid (HONO) that may be occurring within power-plant stacks or immediately after emission. The P6 parameterization also does not account for aqueous-phase oxidation of SO_2 or in-cloud aerosol processing. This missing oxidation pathway would lead to an underestimation of the fraction of SO_2 oxidized on the sub-grid scale. However, little new-particle formation would be predicted under cloudy conditions because of the suppression of sunlight, which in turn would lead to lower OH concentrations and lower H_2SO_4 concentrations (Stevens et al., 2012). We therefore do not expect this missing oxidation pathway to strongly affect predictions of aerosol number. Finally, condensational growth due to SOA within sulphur-rich plumes is not accounted for, which we will discuss further in Sect. 3. We note that at the grid-resolved scale, the GEOS-Chem-TOMAS model does represent aqueous oxidation of SO_2, in-cloud aerosol processing, and condensational growth of aerosol due SOA. Despite the limitations listed above, the SAM-TOMAS model has been shown to predict well the number and size of aerosol formed in coal-fired power plant plumes (Stevens et al., 2012; Lonsdale et al., 2012). We therefore expect that the variability in new-particle formation and growth rates within sulphur-rich plumes is well represented by the P6 parameterization.

Because the emissions inventories used by GEOS-Chem do not provide source-specific emissions, but instead emissions summed across a $1° \times 1°$ grid, the distance downwind from the source is not calculable. We therefore use a length scale equal to half of the square root of the grid
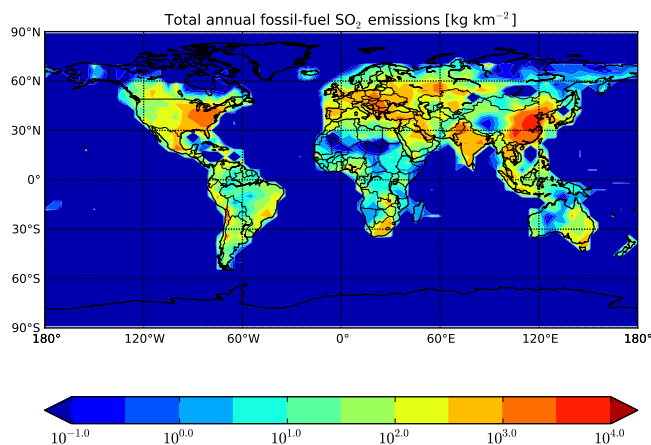
Figure 1. Total annual fossil-fuel SO_2 emissions in $kg\,km^{-2}$ used for this study, excluding shipping emissions.

cell horizontal area, as suggested in Stevens and Pierce (2013), for the distance from the source (d) required for P6. In GEOS-Chem-TOMAS, the value of the boundary-layer height (BLH) used as input to P6 is based on BLH values from the GEOS-5 reanalysis. We note that the BLH values from the GEOS-5 reanalysis were found to be unrealistically low under night-time conditions, and therefore the boundary-layer heights within GEOS-Chem-TOMAS used as input to P6 have been adjusted from the original GEOS-5 reanalysis values by limiting them to a minimum of the mechanical mixing depth, which is calculated based on the local friction velocity (Heald et al., 2012; Walker et al., 2012). We also note that the BLH values were defined within the GEOS-5 dataset as the height where the diffusivity falls below a critical value (Rienecker, 2006). The BLH values used to create the P6 parameterization came from the North American Regional Reanalysis dataset, where they were defined as the height where the turbulent kinetic energy falls below a critical value (Mesinger et al., 2006), and these values may differ due to the different definitions. However, of the nine inputs to the P6 parameterization, the BLH is the input to which all outputs of P6 have the weakest sensitivity (Stevens and Pierce, 2013). We therefore do not expect that uncertainties in BLH values will have a large impact on our results. We also make the following assumption about the sizes of individual sources, as recommended in Stevens and Pierce (2013): We assume that within each model grid cell, the SO_2 emissions are split between an equal number of low emitters, medium emitters, and high emitters. We define high emitters, medium emitters, and low emitters based on the emissions data for power-plants in the United States compiled from the Clean Air Markets (CAM) data (United States Environmental Protection Agency, 2012) as follows: For medium emitters, we use the log-space mean emission rates for a power plant in the USA during 2010. For low and high emitters, we use an emission rate that is one stan-

dard deviation below or above the mean in log space, respectively. The low, medium, and high emission rates of SO_2 are $0.0606\,kg\,s^{-1}$, $0.202\,kg\,s^{-1}$, and $1.00\,kg\,s^{-1}$, respectively. We further assume that the low, medium, and high emitters emit $0.0300\,kg\,N\,s^{-1}$, $0.0840\,kg\,N\,s^{-1}$, and $0.290\,kg\,N\,s^{-1}$ of NO_x, derived in the same way from the 2010 EPA CAM NO_x emissions data.

We performed 19 simulations with GEOS-Chem-TOMAS, summarized in Table 1 and described below. All simulations were performed with meteorology and emissions for the year 2005. Simulations labelled NoSGS did not include any sub-grid sulphate emissions. Simulations labelled AS3 emitted 3 % of anthropogenic SO_2 as sub-grid sulphate, using the bi-modal size distribution described in Adams and Seinfeld (2003) comprised of a nucleation mode containing 15 % of the emitted sulphate mass with a 10 nm number median diameter and a geometric standard deviation of 1.6; and an Aitken mode containing the rest of the sulphate mass with a 70 nm number median diameter and a geometric standard deviation of 2.0. Simulations labelled LY5 emitted 5 % of anthropogenic SO_2 as sub-grid sulphate, emitting 5 % of the sulphate into the same nucleation mode as AS3, but the remaining sulphate was condensed onto pre-existing aerosol, as was done for one of the simulations described in Luo and Yu (2011). Simulations labelled P6 used the P6 parameterization to predict the fraction of anthropogenic SO_2 to emit as sub-grid sulphate, as well as the fraction of the emitted sulphate to emit as particles or condense onto pre-existing particles, and the size of the emitted particles. The amount of sub-grid sulphate emitted and the size of the particles emitted therefore varied with each time step and with each model grid cell in simulations labelled P6.

Secondary organic aerosol (SOA) production in TOMAS is calculated as 10 % of global monoterpene emissions (based on MEGAN, (Guenther et al., 2006)), resulting in approximately $19\,Tg\,yr^{-1}$ of SOA. However, the study of Spracklen et al. (2011) suggested that including emissions of an additional $100\,Tg\,yr^{-1}$ of SOA co-located with anthropogenic pollution yields much better agreement of organic aerosol mass with Aerosol-Mass-Spectrometer-based observations. This additional source of "anthropogenically controlled" SOA has been implemented into GEOS-Chem-TOMAS previously (D'Andrea et al., 2013), where it was also found to provide much better agreement with size distribution observations. This SOA is condensed irreversibly to the Fuchs-corrected aerosol surface area as this was shown to give the best agreement with size distributions in D'Andrea et al. (2013). Simulations labelled "yXSOA" therefore contain additional emissions of $100\,Tg\,yr^{-1}$ of SOA co-located with anthropogenic CO emissions. Simulations labelled "nXSOA" do not contain these additional emissions. One limitation of our yXSOA simulations is that the extra SOA does not aid in the sub-grid nucleation and growth as the P6 scheme does

not handle sub-grid growth from SOA. The implications of this will be discussed in the results section.

Binary ($H_2SO_4 + H_2O$) nucleation rates were predicted in all simulations by the classical binary nucleation scheme described by Vehkamäki et al. (2002). In addition to binary nucleation, ternary ($H_2SO_4 + NH_3 + H_2O$) nucleation was predicted in simulations labelled "Napa" by the parameterization of ternary homogeneous nucleation of sulphuric acid, ammonia and water described by Napari et al. (2002) scaled down globally by a constant factor of 10^{-5} which has been shown to predict nucleation rates closer to measurements than other commonly used nucleation schemes (Jung et al., 2010; Westervelt et al., 2013, 2014). Within simulations labelled "Act", nucleation in the boundary layer was predicted using activation-type nucleation, and ternary nucleation was shut off (binary nucleation was left on). The nucleation rate in activation-type nucleation simulations was a linear function of sulphuric acid concentration, according to the following equation (Kulmala et al., 2006; Sihto et al., 2006):

$$J = 2 \times 10^{-6}\ [H_2SO_4]$$

where J is the nucleation rate and the units of the prefactor are s^{-1}. All nucleation schemes used in this study predict the formation rate of 1 nm particles. Aerosol growth and coagulational loss below 3 nm is approximated by the parameterization of Kerminen and Kulmala (2002).

Lonsdale et al. (2012) showed that the average emissions rate of SO_2 from US coal-fired power plants decreased by 36 % from 1997 to 2010, and that the emissions rate of NO_x decreased by 52 % from 1997 to 2010. These decreases were achieved primarily through the implementation of pollution-control technologies or switching to coal with lower sulphur contents. In order to assess the potential effect of such pollution controls on sub-grid sulphate formation, we performed three additional simulations with nucleation and SOA assumptions the same as the P6_nXSOA_Napa simulation. Simulation P6_hiSO2 differs from the P6_nXSOA_Napa simulation only in that both the assumed SO_2 emissions used as input to P6 and the modelled fossil-fuel emissions of SO_2 (excluding those from shipping) are increased globally by 50 %. We note that real-world SO_2 emissions were not greater in the past for all locations globally, and the SO_2 emissions in this simulation are therefore not meant to represent any previous year but rather a general sensitivity to these emissions. Similarly, in simulation P6_hiNOx, both the assumed emissions of NO_x used as input to P6 and the modelled fossil-fuel NO_x emissions are increased globally by 50 %. We note that NO_x pollution controls have not been implemented globally, and that fossil-fuel NO_x emissions include other sources than coal-fired power plants, such as vehicular exhaust. However, the available inventories for anthropogenic NO_x do not separate coal-fired power plants from other anthropogenic sources, and it is beyond the scope of this paper to estimate what proportion of anthropogenic NO_x emissions are due to coal-fired power-plant emissions.

Table 1. Summary of GEOS-Chem-TOMAS simulations performed. The different sub-grid sulphate schemes and nucleation schemes are further described in Sect. 2. Extra SOA refers to emissions of $100\,\mathrm{Tg\,yr^{-1}}$ of SOA, co-located with emissions of CO.

Name	Sub-grid sulphate	Extra SOA	Boundary-layer nucleation	Changes to emissions
NoSGS_yXSOA_Napa	none	on	Ternary	–
NoSGS_yXSOA_Act	none	on	Activation	–
NoSGS_nXSOA_Napa	none	off	Ternary	–
NoSGS_nXSOA_Act	none	off	Activation	–
AS3_yXSOA_Napa	AS3[1]	on	Ternary	–
AS3_yXSOA_Act	AS3	on	Activation	–
AS3_nXSOA_Napa	AS3	off	Ternary	–
AS3_nXSOA_Act	AS3	off	Activation	–
LY5_yXSOA_Napa	LY5[2]	on	Ternary	–
LY5_yXSOA_Act	LY5	on	Activation	–
LY5_nXSOA_Napa	LY5	off	Ternary	–
LY5_nXSOA_Act	LY5	off	Activation	–
P6_yXSOA_Napa	P6[3]	on	Ternary	–
P6_yXSOA_Act	P6	on	Activation	–
P6_nXSOA_Napa	P6	off	Ternary	–
P6_nXSOA_Act	P6	off	Activation	–
P6_hiSO2	P6 ($E_{SO_2} \times 1.5$)	off	Ternary	$SO_2 \times 1.5$
P6_hiNOx	P6 ($E_{NO_x} \times 1.5$)	off	Ternary	$NO_x \times 1.5$
P6_hiboth	P6 ($E_{SO_2} \times 1.5$ and $E_{NO_x} \times 1.5$)	off	Ternary	$SO_2 \times 1.5$ and $NO_x \times 1.5$

[1] AS3 – 3 % of SO_2 emitted as sub-grid sulphate, 15 % of sub-grid sulphate emitted into nucleation mode and remaining sub-grid sulphate emitted into Aitken mode.

[2] LY5 – % of SO_2 emitted as sub-grid sulphate, 5 % of sub-grid sulphate emitted into nucleation mode and remaining sub-grid sulphate condensed onto pre-existing aerosol.

[3] P6 – fraction of SO_2 emitted as sub-grid sulphate, number and size of sub-grid sulphate particles dynamically predicted by P6 parameterization, remaining sub-grid sulphate condensed onto pre-existing aerosol.

The NO_x emissions in simulation P6_hiNOx are therefore not representative of any past year, and again are for general sensitivity purposes only. Simulation P6_hiboth includes increased emissions of SO_2 used as input to P6 and increased emissions of fossil-fuel SO_2 by 50 %, as well as increased assumed NO_x emissions used as input to P6 and increased fossil-fuel NO_x emissions by 50 %.

3 Sensitivity to sub-grid sulphate scheme

We present the relative changes in globally and annually averaged boundary-layer N3, N10, N40 and N80 due to sub-grid sulphate in Table 2. The values in the table are calculated by comparing each listed simulation with the corresponding simulation that had no sub-grid sulphate, the same amount of SOA emissions, and the same grid-resolved nucleation scheme. We exclude from Table 2 the emissions sensitivity studies, which will be discussed in Sect. 5.

The simulations with AS3 sub-grid sulphate have decreases in N3, but increases in N10, N40, and N80 (Table 2). As the median diameter of the AS3 nucleation mode is 10 nm, the added particles are sufficiently large to provide an additional coagulation sink for the smallest particles resolved by GEOS-Chem-TOMAS, and increased competition for H_2SO_4, which somewhat suppresses new-particle forma-

tion. These feedbacks result in a decrease in the number of particles smaller than 10 nm, but increases in particle number concentrations at larger sizes.

In Fig. 2 we show the changes in annually averaged boundary-layer N80 between the four AS3 simulations and the corresponding simulations with no sub-grid sulphate. Regardless of SOA amount and grid-resolved nucleation scheme, the inclusion of AS3 sub-grid sulphate increases N80 over industrialized regions. However, the two simulations that include anthropogenically controlled SOA (yXSOA, panels a and c) show a greater increase in N80, especially over the Northern Hemisphere. In these simulations, the newly formed sub-grid sulphate particles grow more quickly due to the condensation of the additional SOA mass, and a greater fraction grow larger than 80 nm. This is consistent with the findings of D'Andrea et al. (2013), where including an additional $100\,\mathrm{Tg\,yr^{-1}}$ of SOA was found to increase globally and annually averaged boundary-layer N80 by 29.9 %. The increased survivability of the sub-grid sulphate particles can also be seen in the N3, N10 and N40 changes (Table 2). The two AS3 simulations with anthropogenically controlled SOA show smaller decreases in N3 and larger increases in N10 and N40 from the corresponding no sub-grid sulphate cases than the AS3 simulations without this extra source of SOA.

Table 2. Changes in globally, annually averaged N3, N10, N40 and N80 attributable to sub-grid sulphate emissions. Each simulation is compared to the NoSGS case with the same SOA emissions and the same grid-resolved nucleation scheme.

Simulation	% change in N3	% change in N10	% change in N40	% change in N80
AS3_yXSOA_Napa	−0.36	+8.93	+11.67	+9.73
LY5_yXSOA_Napa	+5.21	+24.17	+25.17	+19.72
P6_yXSOA_Napa	−13.57	−9.09	−3.72	−0.86
AS3_nXSOA_Napa	−3.71	+4.44	+5.32	+4.94
LY5_nXSOA_Napa	−9.51	+3.91	+11.27	+10.78
P6_nXSOA_Napa	−18.34	−12.97	+0.32	+3.46
AS3_yXSOA_Act	−0.50	+4.40	+9.90	+8.43
LY5_yXSOA_Act	+1.05	+13.86	+23.72	+19.11
P6_yXSOA_Act	−2.69	−2.83	−0.45	+1.32
AS3_nXSOA_Act	−1.41	+3.17	+4.52	+4.07
LY5_nXSOA_Act	−3.48	+4.48	+11.90	+10.56
P6_nXSOA_Act	−5.86	−4.87	+3.80	+5.71
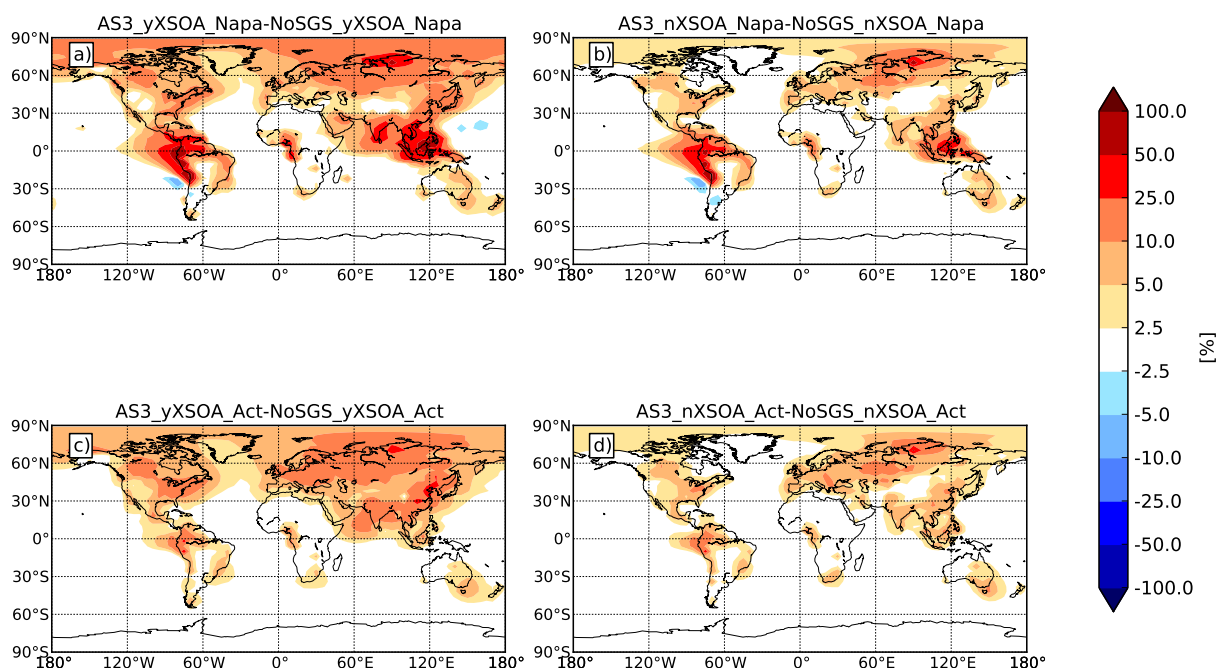
Figure 2. Change in annually averaged boundary-layer N80 between the AS3 simulations and the NoSGS simulations for the **(a)** yXSOA_Napa, **(b)** nXSOA_Napa, **(c)** yXSOA_Act, and **(d)** nXSOA_Act cases.

The two AS3 simulations with ternary nucleation (Napa) show a much greater increase in N80 over north-western South America and the Malay Archipelago. In these regions, little ammonia is present, so less nucleation is predicted by the ternary nucleation scheme than the activation nucleation scheme. Therefore, when no sub-grid sulphate is included, the simulations with activation-type nucleation (Act) have higher N80 in these regions than the simulations with ternary nucleation, and so the addition of a fixed amount of sub-grid sulphate causes a smaller relative change in N80 for the activation-type nucleation simulations than the ternary nucleation simulations in these regions.

The changes in N80 between simulations with LY5 sub-grid sulphate and the corresponding simulations with no sub-grid sulphate (not shown) are similarly distributed spatially to those from the AS3 simulations, but greater in magnitude (see Table 2). The effects of changing SOA amount and grid-resolved nucleation scheme are also similar for the LY5 simulations. The increase in the magnitude of the changes in N80 for the LY5 simulations relative to the AS3 simulations is in part due to the greater fraction of SO_2 that is assumed to be

oxidized on the sub-grid scale (5 % for LY5, compared to 3 % for AS3). In addition, while both AS3 and LY5 sub-grid sulphate use the same size distribution for nucleation mode particles, the remaining sulphate mass is emitted as Aitken-mode particles in AS3, whereas the remaining mass is condensed onto pre-existing particles in LY5. In the LY5 simulations, particles emitted into the nucleation mode in one model time step will be grow by sub-grid condensation during following time steps, and this will speed their growth to CCN sizes. In contrast, the Aitken-mode particles emitted in simulations using the AS3 sub-grid sulphate scheme will remove nucleation-mode particles in subsequent time steps through coagulation. Because of these effects, the LY5 scheme more efficiently produces CCN-sized particles.

We note that the LY5 simulations with anthropogenically controlled SOA are the only simulations that show an increase in N3 compared to the simulations without sub-grid sulphate (Table 2). As the nucleation-mode sub-grid sulphate is still being emitted with median diameter 10 nm, as in the AS3 simulations, one would expect a decrease in the number of sub-10 nm particles, as was seen for the AS3 simulations. Through inspection of globally averaged size distributions (not shown), we have determined that the number of sub-10 nm particles decreases in these simulations as well, but the increases in N10 are sufficiently large to more than compensate for these decreases, resulting in a net increase in N3.
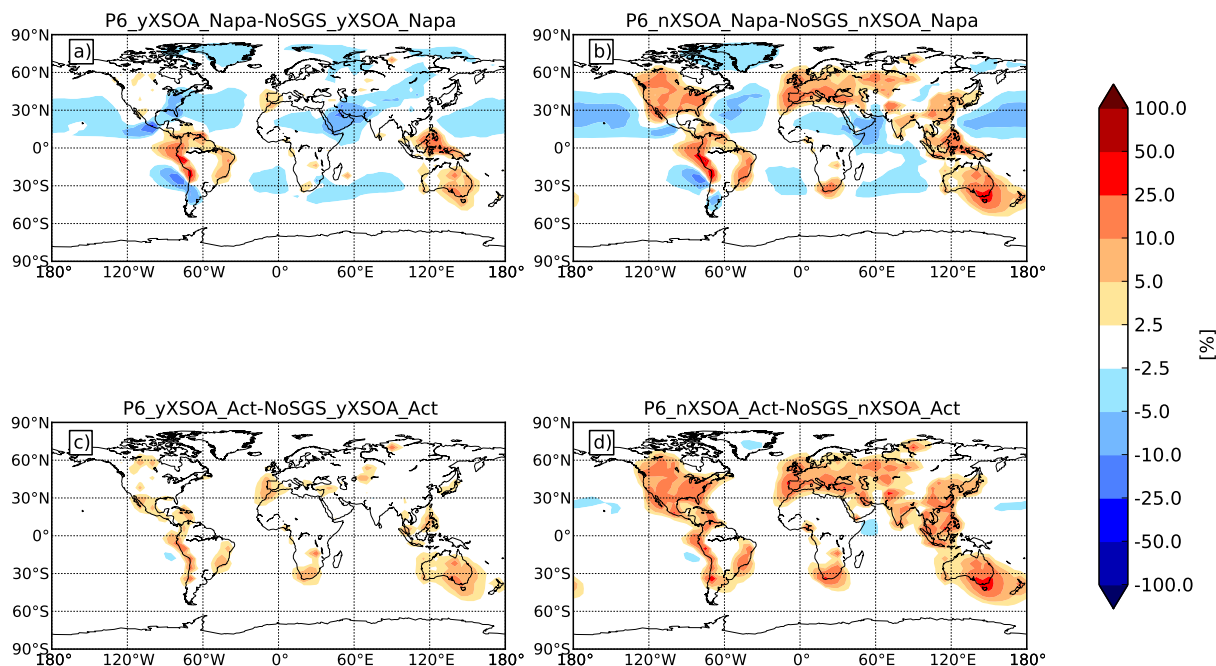
Figure 3 shows the change in annually averaged N80 between the four P6 simulations and the corresponding simulations without sub-grid sulphate. In contrast to the AS3 and LY5 simulations, the enhancement in N80 due to sub-grid sulphate for the P6 simulations is smaller for the simulations where anthropogenically controlled SOA is included (yX-SOA, panels a and c) than for the two simulations without this extra source of SOA (nXSOA, panels b and d). Notably, in the simulations with anthropogenically controlled SOA and ternary nucleation, globally, annually averaged N80 is less when using P6 sub-grid sulphate than with no sub-grid sulphate (P6_yXSOA_Napa vs. NoSGS_yXSOA_Napa), as shown in Fig. 3a and listed in Table 2. We will show in the following section that the additional SOA increases the pre-existing condensation sink, which in turn causes P6 to predict much less sub-grid new-particle formation and growth. However, higher concentrations of SOA would be expected to condense onto newly formed particles at the sub-grid scale as well as at the grid-resolved scale, which would increase the growth and survivability of the newly formed particles. It has been shown that SOA may preferentially form within anthropogenic plumes (Carlton et al., 2009, 2010; D'Andrea et al., 2013; Heald et al., 2011; Offenberg et al., 2009; Spracklen et al., 2011; Surratt et al., 2007), which may imply that SOA preferentially condenses onto particles within sulphur-rich plumes, compared to particles outside of such plumes. These processes would compensate somewhat for the suppression of new-particle formation by the enhanced background con-

densation sink, but are not currently accounted for by the P6 parameterization because the mechanism(s) for the formation of this anthropogenically controlled SOA remain poorly understood. It is therefore possible that sub-grid new-particle formation and growth is under-predicted by the P6 parameterization for the cases with anthropogenically controlled SOA. We intend to include the effects of this SOA on sub-grid formation and growth in a future version of the P6 parameterization, once these processes become better understood.

In panels a and b of Fig. 3 a decrease in N80 is shown over the oceanic regions downwind of polluted regions. This decrease occurs for the two ternary nucleation cases (Napa), but not for the activation-type nucleation cases (Act). The sub-grid condensation of H_2SO_4 in all P6 cases increases the coagulation sink downwind of polluted regions, and the larger particles are more efficiently removed by wet deposition. In the activation-type nucleation simulations, nucleation and growth over the oceanic regions dampen this decrease in N80, but the Napari ternary nucleation scheme predicts little new-particle formation over ocean regions, and the regions of decreased N80 persist. These decreases are even more strongly pronounced for smaller particles, and this effect is responsible for the more negative values of the changes in N3, N10, and N40 in the P6 Napa simulations than the P6 Act simulations, as shown in Table 2.

When anthropogenically controlled SOA is included, the P6 cases show much smaller increases in annually averaged N80 than the AS3 and LY5 cases, particularly in the Northern Hemisphere (see Table 2 and compare Fig. 2, panels a and c with Fig. 3, panels a and c). As mentioned above, the P6 parameterization may be underestimating sub-grid new-particle formation and growth in these cases because it does not include any enhancement of new-particle formation and growth by SOA within the sub-gid plumes. Without this source of SOA, the P6 and AS3 sub-grid sulphate schemes increase globally, annually averaged N80 by a similar amount, while the LY5 sub-grid sulphate scheme increases globally, annually averaged N80 by roughly twice this amount (Table 2). The increases in N80 are spatially distributed somewhat differently in P6 than AS3 and LY5, however (compare Fig. 2, panels b and d with Fig. 3, panels b and d). The AS3 and LY5 sub-grid sulphate schemes increase N80 over the Arctic, but the P6 parameterization predicts little new-particle formation and growth over the Arctic because little sunlight is available at such high latitudes for OH formation and subsequent oxidation of SO_2. Compared to the AS3 cases, this is compensated by increased N80 over eastern North America, South Africa, southeast Australia, Portugal and Spain. The P6 parameterization tends to predict more new-particle formation and growth over these regions due to the relatively greater sunlight and lower condensation sink in these regions (shown in next section). The assumption that the amount and size of sub-grid sulphate formed is constant (e.g. AS3 and LY5) may therefore be unable to resolve im-

Figure 3. Change in annually averaged boundary-layer N80 between the P6 simulations and the NoSGS simulations for the **(a)** yXSOA_Napa, **(b)** nXSOA_Napa, **(c)** yXSOA_Act, and **(d)** nXSOA_Act cases.

portant regional differences in sub-grid new-particle formation and growth.

4 The P6 Gradient Subroutine, and sensitivities to P6 inputs

In order to better understand the results of P6 simulations, including differences between P6 simulations due to SOA amount and emissions, and differences in the P6 simulations from AS3 and LY5 simulations, we have created the P6 Gradient Subroutine. This subroutine allows us to quickly test the sensitivity of the P6 outputs (fraction of emitted SO_2 oxidized to form H_2SO_4 (f_{ox}), fraction of that H_2SO_4 that forms new particles (f_{new}), median diameter of newly formed particles (D_m), and number of newly formed particles per kg SO_2 emitted (N_{new})) to changes in each of the P6 inputs (emissions of SO_2 (E_{SO_2}) and NO_x (E_{NO_x}) from the source, background condensation sink of pre-existing particles (CS), downward shortwave radiative flux (DSWRF), mean boundary-layer wind speed (v_g), boundary-layer height (BLH), distance from the source (d), and mean background concentrations of SO_2 (bgSO_2) and NO_x (bgNO_x)). We can use the subroutine to calculate the derivative of each of the outputs of P6 with respect to each of the inputs of P6 for a given set of inputs. We have run the P6 Gradient Subroutine offline using the monthly-mean values of each of the P6 inputs as output by GEOS-Chem-TOMAS. (While the values from the P6 Gradient Subroutine calculated based on monthly means of the P6 inputs will not be equal to

monthly-means of values calculated based on the instantaneous values of the P6 inputs due to non-linearities in the equations, we do not expect that the differences due to these non-linearities would qualitatively alter any of our analysis below.) We discuss below the results of subroutine applied to simulation P6_nXSOA_Napa. We choose P6_nXSOA_Napa for this discussion because, as noted above, the P6 parameterization does not currently include the effects of anthropogenically controlled SOA on sub-grid new-particle formation and growth, and because the scaled Napari ternary nucleation scheme has been shown to yield results that compare more favourably with observations (Westervelt et al., 2013).

We show in Fig. 4 the annually averaged values of each of the P6 outputs, as calculated offline by the P6 Gradient Subroutine for simulation P6_nXSOA_Napa. (We note that because emissions rates are assumed (e.g. high emitters, medium emitters and low emitters, see Sect. 2) for the purposes of calculating the P6 outputs, we can calculate these outputs even where there are no emissions, such as over oceans. However, since the amount of sub-grid sulphate to be emitted is expressed as a fraction of SO_2 emissions (f_{ox}), no sub-grid sulphate will be emitted in the absence of SO_2 emissions.)

As shown in Fig. 4a, over high-pollution regions, the f_{ox} values calculated offline are generally between 5 and 8 %. This is slightly higher than the 3 and 5 % values assumed by AS3 and LY5, respectively. The value of f_{ox} is generally higher in high-pollution regions, as the background NO_x concentrations in these regions are closer to those optimal
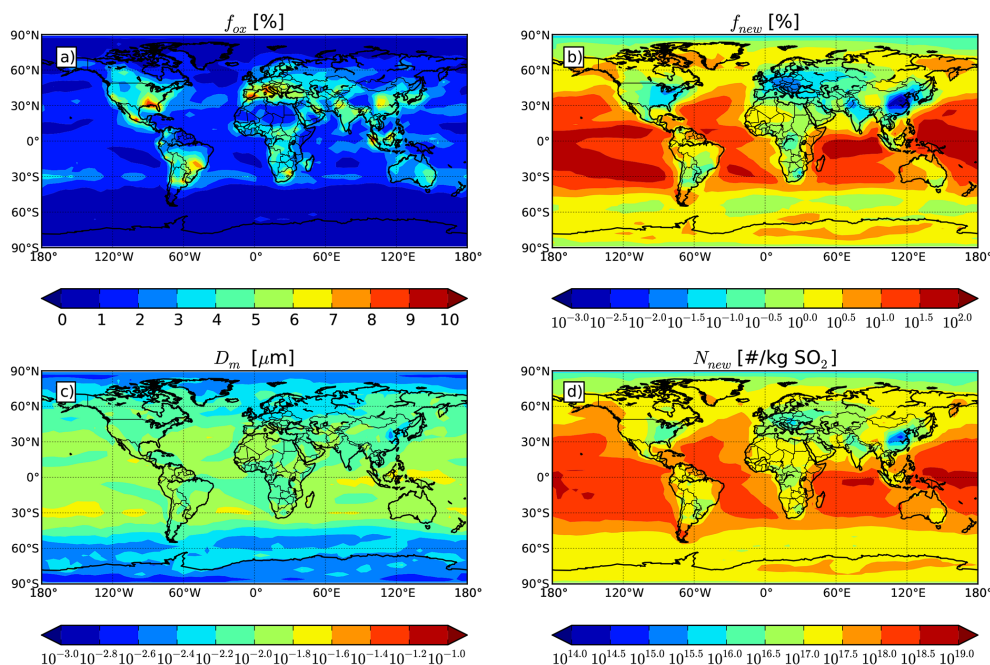
Figure 4. Annually averaged outputs of the P6 parameterization, as calculated offline from monthly-means of the P6 inputs for simulation P6_nXSOA_Napa: **(a)** fraction of emitted SO_2 oxidized (f_{ox}), **(b)** fraction of H_2SO_4 formed that comprises new particles (f_{new}), **(c)** median diameter of emitted particles (D_m), and **(d)** number of new particles per kg SO_2 emitted (N_{new}). We note these values are calculable even in the absence of emissions, see Sect. 4.4.

for OH production, and hence SO_2 oxidation. The value of f_{ox} is commonly lower than 4 % in rural regions, and can fall to less than 1 % in very remote regions with little annually averaged sunlight for photo-oxidation. In contrast f_{new} is much lower over polluted regions, with values less than 0.1 % over the eastern US, Europe, and less than 0.01 % over China. For the LY5 sub-grid sulphate scheme, the value of f_{new} is assumed to be 5 % everywhere. The AS3 sub-grid sulphate scheme emits 15 % of sulphate into the nucleation mode, and while this is not directly comparable to f_{new} in the P6 scheme (since the remaining sulphate in AS3 is emitted into the Aitken mode and not condensed onto pre-existing particles), both the AS3 and LY5 schemes assume a far greater proportion of sub-grid sulphate forms new particles than is predicted by the P6 parameterization over high-pollution regions. As a much smaller fraction of sub-grid sulphate forms new particles in the simulations using the P6 scheme, there are many fewer particles available to grow to CCN sizes, and hence generally a smaller change in N80 from the simulations without sub-grid sulphate. For the P6 case with anthropogenically controlled SOA and ternary nucleation (P6_yXSOA_Napa), the growth of pre-existing particles by this sub-grid condensation allows them to more effectively remove particles through coagulation resulting in a decrease in N80 from the corresponding case with no sub-grid sulphate (NoSGS_yXSOA_Napa).

In Fig. 5 we show the annually averaged sensitivity of N_{new} to each of the P6 inputs for simulation

P6_nXSOA_Napa, as the percentage change in N_{new} for a percentage change in the input. For each latitude and longitude point, we exclude months where no nucleation would be predicted based on the monthly mean of the P6 inputs, as the sensitivity of N_{new} to a change in the P6 inputs is ill-defined for no-nucleation cases. We note that N_{new} and f_{new} are very sensitive to the condensation sink (CS). A 1 % increase in CS yields a decrease in the predicted value of N_{new} of between 1 and 2 % over most locations, and greater decreases over polluted regions such as the eastern United States, Europe, India and China (Fig. 5). A 1 % increase in CS also yields a decrease in the predicted values of f_{new} of more than 2 % over polluted regions (not shown). We show in Fig. 6 the difference in CS between simulations NoSGS_yXSOA_Napa and NoSGS_nXSOA_Napa, to show the change in CS due to the extra SOA. Figure 6 shows that inclusion of the anthropogenically controlled SOA increases CS by more than 75 % over most of the continental Northern Hemisphere, and increases CS by more than 100 % over most of North America and Europe. We would therefore expect much lower values of N_{new} and f_{new} in these regions. The decreased value of N_{new} would result in the formation of fewer new particles that could potentially grow to CCN sizes. A much greater fraction of the sub-grid-oxidized SO_2 would also be expected to condense onto pre-existing particles, further increasing the condensation sink and suppressing further new-particle formation, both at the grid-resolved scale and the sub-grid scale. Together, these processes are responsible for a drastic reduc-

% ΔN_{new} / % Δ input
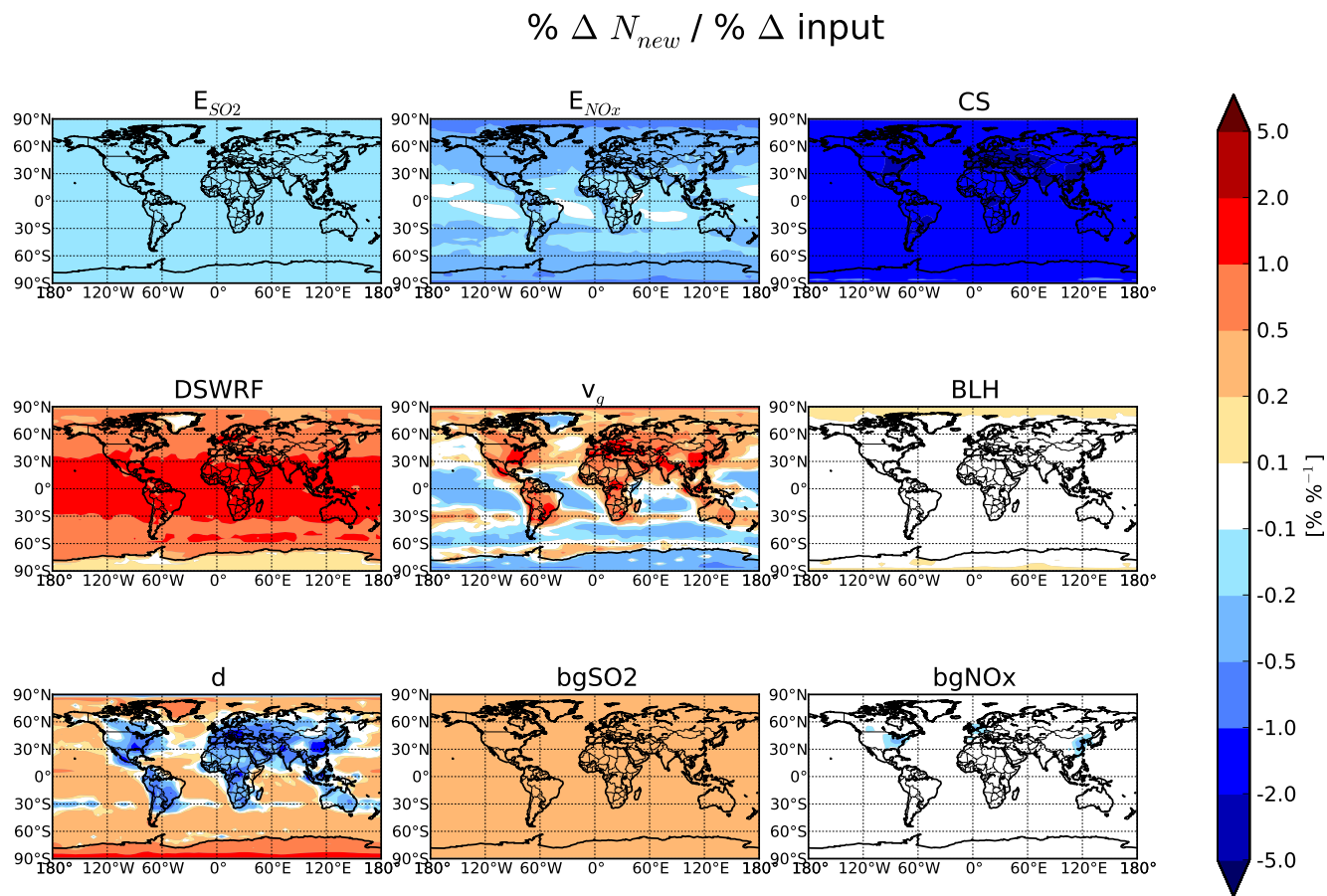
Figure 5. Annually averaged sensitivity of N_{new} to each of the inputs to P6 for simulation P6_yXSOA_Napa, given as the percentage change in the value of N_{new} for a percentage change in the value of the input.
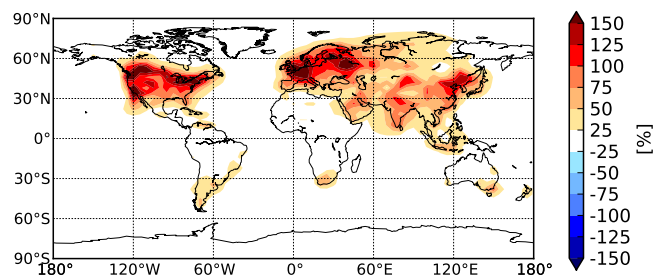
Figure 6. Change in annually averaged condensation sink between NoSGS_yXSOA_Napa and NoSGS_nXSOA_Napa.

tion in the number of sub-grid sulphate particles that may grow to CCN sizes when anthropogenically controlled SOA is included. However, as noted in the previous section, anthropogenically controlled SOA would be expected to condense onto newly formed particles at the sub-grid scale, but sub-grid condensation of SOA is not currently resolved by P6. Since anthropogenically controlled SOA may preferentially form within coal-fired power-plant plumes, it is likely that the enhanced growth of newly formed particles by this

SOA would offset to some extent the suppression of new-particle formation and growth shown by our results.

5   Effects of pollution controls

As described in Sect. 2, we performed additional simulations in order to test the effects of pollution controls upon our results. The simulations P6_hiSO2, P6_hiNOx, and P6_hiboth differ from P6_nXSOA_Napa only in that the emissions of SO2, NOx, or both SO2 and NOx have been increased by 50 %. Emissions of sub-grid sulphate in the P6 sub-grid sulphate scheme (and both other sub-grid sulphate schemes used in this study) are normalized by the modelled emissions of SO2. Consequently, the emissions of sub-grid sulphate would be increased by 50 % in the P6_hiSO2 and P6_hiboth simulations if the P6 outputs remained constant. The differences in globally, annually averaged N3, N10, N40, and N80 between the P6_hiSO2, P6_hiNOx, and P6_hiboth simulations and the P6_nXSOA_Napa simulation are shown in Table 3, and the differences in annually averaged N80 are shown in Fig. 7. The globally, annually averaged N80 in simula-

Table 3. Changes in globally, annually averaged N3, N10, N40 and N80 due to 50 % increases in emissions from the P6_nXSOA_Napa simulation. Decreases in N3 for the P6_hiSO2 and P6_hiboth cases are due primarily to enchanced coagulation. Increases in N40 and N80 for P6_hiSO2 and P6_hiboth are due primarily to enhanced condensational growth. Increases at all sizes for the P6_hiNOx case are due to enchanced grid-resolved nucleation and growth.

| Simulation	% change in N3	% change in N10	% change in N40	% change in N80
P6_hiSO2	−8.18	−0.68	+7.35	+9.00
P6_hiNOx	+0.61	+2.04	+2.22	+1.47
P6_hiboth	−8.14	+0.80	+9.26	+10.24
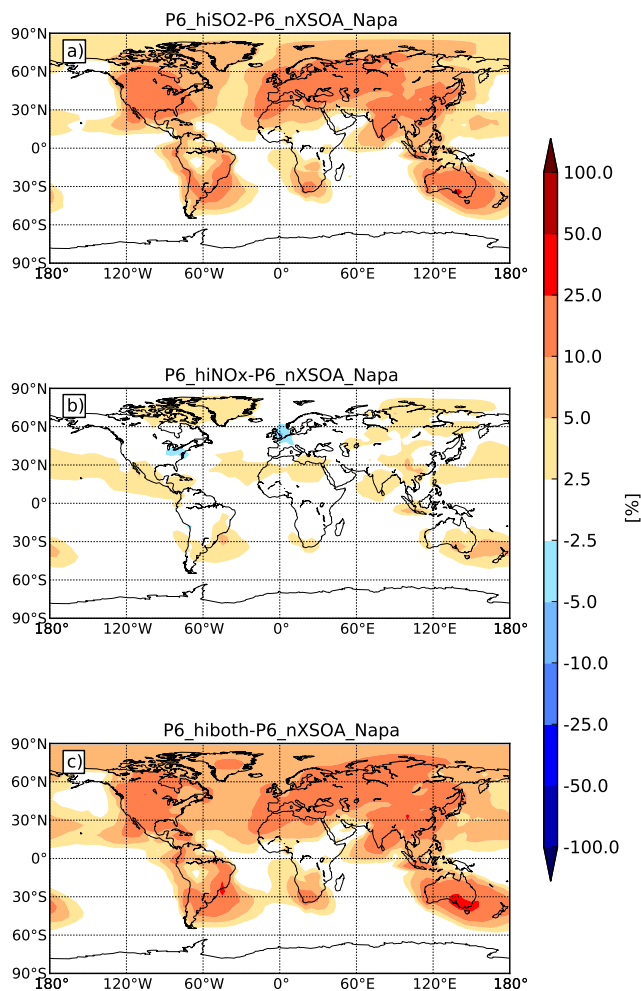
Figure 7. Change in annually averaged N80 between **(a)** P6_hiSO2, **(b)** P6_hiNOx, **(c)** P6_hiboth and P6_nXSOA_Napa.

tions P6_hiSO2, P6_hiNOx, and P6_hiboth increase from the P6_nXSOA_Napa simulation by 9.00, 1.47, and 10.24 %, respectively. Greater SO_2 emissions increase new-particle formation and growth through the additional source of sulphate, at both the grid-resolved and sub-grid scales. Greater NO_x concentrations in the P6_hiNOx and P6_hiboth simulations allow for greater OH production and faster oxidation of SO_2,

at both the grid-resolved and sub-grid scales, except in the most polluted regions.

The increases in the assumed emissions of SO_2 (E_{SO_2}) and NO_x (E_{NO_x}) used as input to P6 will alter the values of the P6 outputs, and hence the number and size of sub-grid sulphate formed in the emissions sensitivity simulations. Increases in the background concentrations of SO_2 (bgSO_2) and NO_x (bgNO_x) in the P6_hiSO2 and P6_hiNOx simulations, respectively, will lead to differences in the P6 outputs. The changes in sulphate formation and growth (at both the grid-resolved and sub-grid scales) due to increased bgSO_2 and bgNO_x will result in changes to the grid-resolved aerosol condensation sink (CS), which will also influence the P6 outputs. We have used the P6 Gradient Subroutine to estimate the differences in the annually averaged P6 outputs between the P6_hiSO2, P6_hiNOx, and P6_hiboth simulations, and the P6_nXSOA_Napa simulation (Fig. 8). The fraction of SO_2 oxidized (f_{ox}) in the P6_hiSO2 simulation does not significantly differ from that of the P6_nXSOA_Napa simulation (Fig. 8a), as f_{ox} is not sensitive to E_{SO_2}, bgSO_2, or CS. The number of new particles formed per kg SO_2 emitted (N_{new}) in P6_hiSO2 generally decreases by 20–30 % over polluted regions (Fig. 8b) due to an increase in the condensation sink. However, since N_{new} is normalized by SO_2 emissions, which are increased by 50 % in this simulation, there would still be a net increase in the absolute number of sub-grid sulphate particles formed on the sub-grid scale. In order to demonstrate the net change in the absolute number of sub-grid particles formed, including the 50 % increase due to the 50 % increase in SO_2 emissions, we plot the relative difference between $N_{new} \cdot 1.5$ from the P6_hiSO2 and P6_hiboth simulations and the value of N_{new} in the P6_nXSOA_Napa simulation in Fig. 9. In simulation P6_hiSO2 (Fig. 9a), it is only over eastern China that there is a net decrease in the absolute number of sub-grid sulphate particles formed, even after accounting for the 50 % increase in the number of sub-grid sulphate particles emitted due to the additional SO_2 emissions. This decrease in the absolute number of sub-grid particles formed is due to the increased SO_2 emissions greatly increasing the condensation sink in eastern China (not shown). The median diameter of newly formed particles (D_m) in simulation P6_hiSO2 increases by 13–16 % over most of the globe (Fig. 8c). Therefore, both the num-
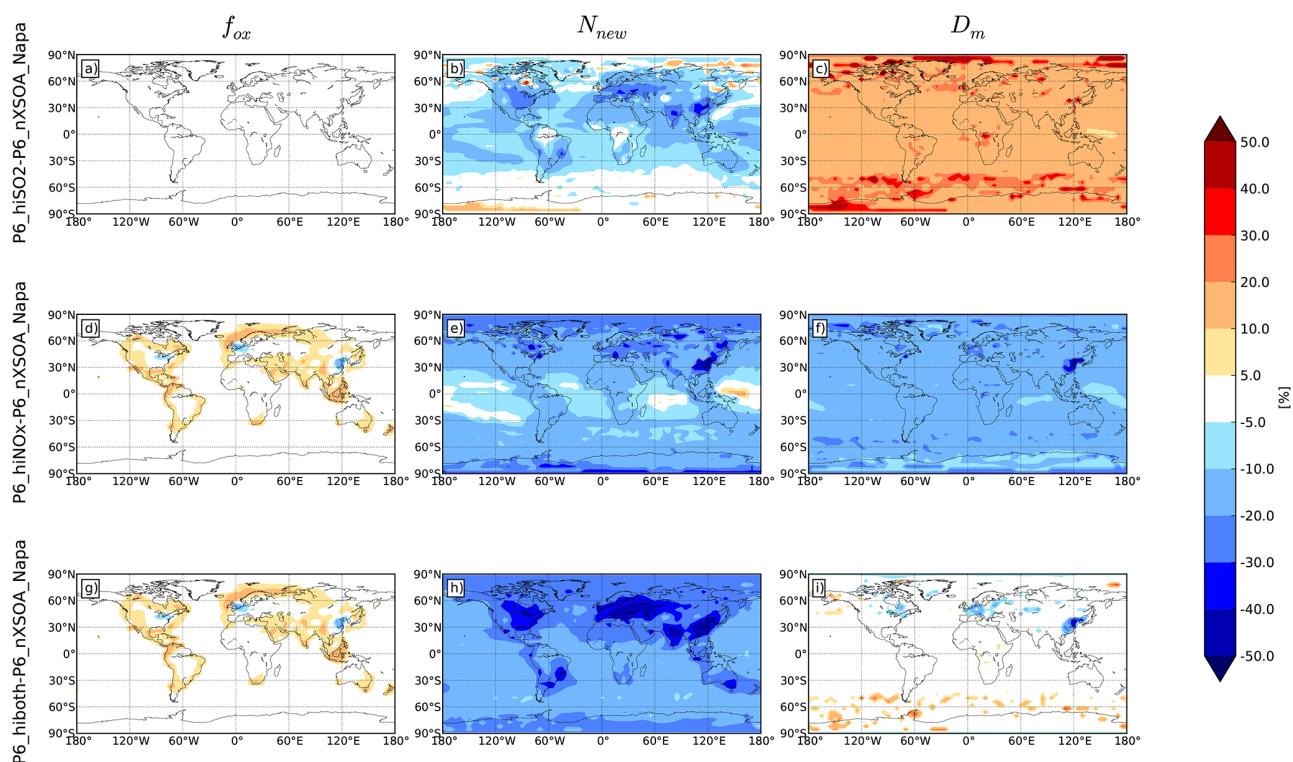
Figure 8. Relative changes in the fraction of SO_2 oxidized on the sub-grid scale (f_{ox}), number of newly formed sub-grid sulphate particles per kg SO_2 emitted (N_{new}), and median diameter of sub-grid sulphate particles (D_m) from the P6_nXSOA_Napa simulation to the P6_hiSO2, P6_hiNOx, and P6_hiboth simulations, as calculated offline by the P6 Gradient Subroutine.

ber and the size of sub-grid sulphate particles are larger in the P6_hiSO2 simulation, and the increased particle number concentrations in this simulation are due in part to changes in sub-grid processes.

The value of f_{ox} in the P6_hiNOx simulations decreases over very polluted regions and increases over remote regions (Fig. 8d), but these relative changes are less than 20 % (or an absolute change in f_{ox} of 1 %) in either direction. Whether f_{ox} decreases or increases depends on the NO_x concentrations in the region. In high-NO_x regimes, in-plume OH concentrations (and hence SO_2 oxidation) will decrease with increasing NO_x, and oxidation will increase with increasing NO_x in low-NO_x regimes. The value of N_{new} in P6_hiNOx decreases by 10–20 % over most of the globe, with greater decreases over Europe and China (Fig. 8e). The value of D_m decreases by 11–14 % over most of the globe (Fig. 8f). These increases in f_{ox} and decreases in N_{new} and D_m will result in more sub-grid oxidation of SO_2, but fewer and smaller new particles emitted at the sub-grid scale. Hence, the only change in sub-grid sulphate that may contribute to the modelled increase in N80 (Fig. 7b) is an increase in condensation of sub-grid-oxidized SO_2 onto pre-existing particles less than 80 nm in diameter. It is therefore likely that the increases in N80 in this simulation are primarily due to grid-resolved processes.

In the P6_hiboth simulation, the changes in f_{ox} (Fig. 8g) are nearly identical to the changes for the P6_hiNOx simulation. The changes in D_m due to increased SO_2 and increased NO_x nearly cancel each other over most of the globe (Fig. 8i), with some exceptions: D_m decreases over eastern Canada, over Europe, and over Eastern China, and it increases over some regions where no anthropogenic sulphur (and hence no sub-grid sulphate) is emitted. The value of N_{new} decreases, as it did for both the P6_hiSO2 and P6_hiNOx simulations. However, the reduction in N_{new} is sufficiently large over polluted regions, including eastern North America, Europe, India, and China, to result in a net reduction in sub-grid new particle formation, even after accounting for a 50 % increase due to the 50 % increase in emissions of SO_2 (Fig. 9b). Over the most polluted regions, increased SO_2 and NO_x emissions therefore result in fewer and smaller sub-grid sulphate particles emitted and a smaller fraction of SO_2 oxidized on the sub-grid scale. However, in less polluted regions the increased SO_2 and NO_x emissions result in the emission of more sub-grid sulphate particles and enhanced sub-grid oxidation of SO_2. Changes in sub-grid sulphate are therefore not uniform with respect to changing emissions when the effects of those emissions on grid-resolved SO_2, NO_x, and aerosol condensation sink are included. These results are consistent with Lonsdale et al. (2012), where they found that NO_x and
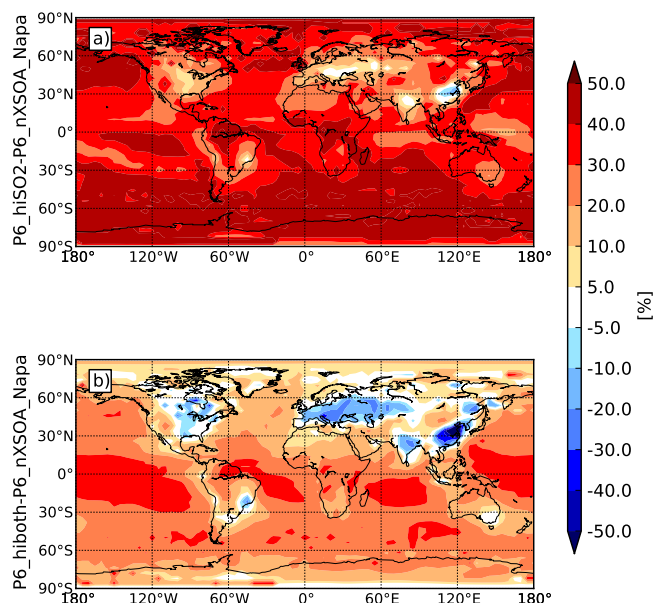
Figure 9. Relative change in the absolute number of newly formed sub-grid sulphate particles (including increases due to increases in SO₂ emissions) from the P6_nXSOA_Napa simulation to the **(a)** P6_hiSO2 and **(b)** P6_hiboth simulations, as calculated offline by the P6 Gradient Subroutine.

SO$_2$ emissions controls may increase or decrease the number of particles in the plume depending on the background NO$_x$ regime, background condensation sinks as well as how strongly NO$_x$ and SO$_2$ are controlled.

6 Comparison with observations

In order to assess the sub-grid sulphate schemes simulated in our study, we used data from the 21 surface-based aerosol size distribution measurements compiled by D'Andrea et al. (2013) from the following sources: the BEACHON campaign (Levin et al., 2012), the European Supersites for Atmospheric Aerosol Research (www.eusaar.net, Asmi et al., 2011; Reddington et al., 2011), the RoMANS 2 campaign (instrumentation and site descriptions are same as RoMANS 1 campaign as per Levin et al., 2009), Environment Canada (Leaitch et al., 2013; Pierce et al., 2012; Riipinen et al., 2011), and Kent State University (Erupe et al., 2010; Kanawade et al., 2012). The measurement sites span many terrain types, including forests, mountains, rural sites, arctic sites and coastal sites. However, urban sites were excluded because the 4° × 5° resolution used for this study cannot resolve urban features. All size distribution measurements were obtained using either a Differential Mobility Particle Sizer (DMPS) (Aalto et al., 2001) or a Scanning Mobility Particle Sizer (SMPS) (Wang and Flagan, 1990). For a map of the locations as well as figures showing the size-

distribution comparisons for similar simulations, please see D'Andrea et al. (2013).

For brevity, we do not show the full comparisons at the sites in figures, but we list in Table 4 the log-mean bias (LMB), slope of a linear regression of the logarithms of the values (m), and coefficient of determination (R^2) between the annually averaged N10, N40, N80, and number concentrations of particles larger than 150 nm (N150) for each simulation (excluding the emissions sensitivity tests) and those measured at the 21 surface sites. These statistics evaluate how well the model captures the magnitude and variability across the measurement sites. We do not compare simulated N3 against observations because measurements of particles smaller than 10 nm were not available at most of the surface sites, and we include N150 to show more information about the larger end of the size distribution. Compared to the choice of SOA amount or grid-resolved nucleation scheme, the choice of sub-grid sulphate scheme has a small effect on the goodness-of-fit metrics shown here. The maximum changes in LMB, m, and R^2 between simulations that differ only in sub-grid sulphate scheme are 0.087, 0.109, and 0.030, respectively. Many other uncertain model parameters and processes can also change aerosol number concentrations, such as emissions and deposition rates, and a change in these parameters or processes within the model may affect our goodness-of-fit metrics.

The simulations without sub-grid sulphate and without anthropogenically controlled SOA (NoSGS_nXSOA) are both biased high for N10, and biased low for N40, N80, and N150. For these cases, the inclusion of any of the three sub-grid sulphate schemes considered here increases N40, N80, and N150 at the expense of N10, and therefore decreases the absolute LMB. However, when anthropogenically controlled SOA is included, the simulations without sub-grid sulphate (NoSGS_yXSOA) tend to have small positive biases for each size range (except for the NoSGS_yXSOA_Act N40, which has a small negative bias). The AS3 and LY5 sub-grid sulphate schemes increase aerosol concentrations at all sizes for the cases with anthropogenically controlled SOA, (since the extra SOA enhances survivability of the small particles, as shown by D'Andrea et al., 2013) and so increase this positive bias. The P6 parameterization predicts that a larger fraction of sub-grid sulphate will condense onto pre-existing particles for the cases with this extra SOA due to the increased condensation sink, and so only N150 increases from the NoSGS_yXSOA cases, and N10, N40, and N80 decrease due to enhanced coagulation from the larger aerosol. These decreases lead to a reduction in the absolute LMB from the NoSGS_yXSOA_Napa case to the P6_yXSOA_Napa case for all size ranges except for N150, and only a small increase in the absolute LMB for all size ranges from the NoSGS_yXSOA_Act case to the P6_nXSOA_Act case.

Log-linear regressions for all cases and all size ranges yield slopes less than 1. This is generally due to an overprediction of aerosol number concentrations at the cleaner sites,

Table 4. Log-mean bias (LMB), slope of the log-linear regression (m), and coefficient of determination (R^2) between the simulated annually averaged N10, N40, N80, and N150 and those measured at 21 surface sites. For each group of simulations with the same SOA amount and grid-resolved nucleation scheme, the best statistical result in each column is bolded. For each group of simulations with the same sub-grid sulphate scheme, the best statistical result in each column is italicized.

Simulation	LMB				m				R^2			
	N10	N40	N80	N150	N10	N40	N80	N150	N10	N40	N80	N150
NoSGS_yXSOA_Napa	0.086	*0.018*	0.077	**0.138**	0.813	*0.850*	*0.825*	*0.842*	0.874	**0.893**	***0.863***	*0.784*
AS3_yXSOA_Napa	0.095	0.040	0.102	0.158	0.802	*0.846*	0.824	0.846	0.885	*0.888*	0.856	0.778
LY5_yXSOA_Napa	0.122	0.070	0.131	0.180	**0.857**	***0.881***	**0.846**	**0.856**	**0.890**	0.878	0.846	0.772
P6_yXSOA_Napa	**0.061**	***0.003***	**0.071**	0.142	0.798	*0.846*	*0.827*	*0.849*	0.871	0.892	***0.863***	*0.789*
NoSGS_yXSOA_Act	***0.005***	−0.050	***0.029***	*0.113*	0.658	0.780	0.783	0.825	0.866	*0.897*	0.860	0.779
AS3_yXSOA_Act	*0.030*	***−0.011***	0.067	0.141	0.685	0.803	0.800	0.837	**0.870**	0.883	0.852	0.774
LY5_yXSOA_Act	*0.073*	0.031	0.105	*0.168*	**0.761**	**0.850**	**0.828**	**0.849**	0.858	0.868	0.843	0.769
P6_yXSOA_Act	*−0.007*	−0.056	***0.029***	0.121	0.652	0.779	0.785	0.832	**0.870**	***0.898***	**0.862**	**0.784**
NoSGS_nXSOA_Napa	0.308	−0.050	−0.134	−0.256	***0.963***	0.781	0.661	0.577	0.894	0.853	0.833	0.763
AS3_nXSOA_Napa	0.304	−0.042	−0.121	−0.239	*0.948*	0.779	0.670	0.593	0.897	0.858	0.833	0.757
LY5_nXSOA_Napa	0.283	***−0.026***	***−0.093***	−0.215	*0.937*	**0.800**	**0.695**	0.612	**0.898**	**0.866**	0.831	0.751
P6_nXSOA_Napa	**0.262**	−0.050	−0.111	**−0.215**	*0.927*	0.794	0.693	**0.623**	0.892	0.863	**0.842**	**0.768**
NoSGS_nXSOA_Act	0.203	−0.115	−0.162	−0.262	0.809	0.729	0.644	0.577	*0.907*	0.864	0.836	0.766
AS3_nXSOA_Act	0.206	−0.099	−0.146	−0.244	0.812	0.738	0.657	0.594	*0.907*	0.866	0.833	0.760
LY5_nXSOA_Act	0.195	**−0.079**	**−0.115**	−0.218	**0.813**	**0.764**	**0.682**	0.614	0.905	0.869	0.830	0.753
P6_nXSOA_Act	**0.174**	−0.107	−0.136	−0.219	0.785	0.746	0.671	**0.621**	***0.911***	**0.874**	**0.843**	**0.770**

and an underprediction of aerosol number concentrations at the more polluted sites. To a certain extent, this behaviour is expected due to model resolution effects alone. The cleanest sites will be influenced by pollution within the same grid cell, and local pollution sources that may influence the measurements at the most polluted sites will be diluted to the model resolution. For nearly all combinations of size range, SOA amount and grid-resolved nucleation scheme, the LY5 sub-grid sulphate scheme yields the slope closest to one. The differences in aerosol number concentrations between simulations, while small everywhere, are greatest for polluted sites, which would be expected if anthropogenic sulphate is a strong contributor to particle number concentrations at these sites. The LY5 scheme typically predicts more particles at all sites than any other sub-grid sulphate scheme, as evidenced by the more positive LMB, but these differences are most pronounced at the most polluted sites. Where the LMB is negative, this increase in aerosol number concentrations yields better agreement with measurements at the more polluted sites. Where the LMB is positive, this increase yields a worse agreement with the measurements at the more polluted sites, but a more consistent bias against the measurements across all of the sites.

Regardless of the SOA amount or grid-resolved nucleation scheme used, simulations using P6 sub-grid sulphate had higher R^2 values for N80 and N150 than any other sub-grid sulphate scheme included in this study. For those cases using activation nucleation, the simulations using the P6 scheme had the highest R^2 values for N10 and N40 as well. While this difference is small, we believe that this improved correlation is due to the fact that the P6 parameterization predicts different amounts and sizes of sub-grid sulphate under different conditions, and can therefore represent more spatial heterogeneity than the other sub-grid sulphate schemes tested in this study.

7 Conclusions

In this study, we implemented the P6 parameterization for sub-grid sulphate into the GEOS-Chem-TOMAS global chemical-transport model. This is the first implementation of P6 into a global model. We have shown that the P6 parameterization predicts smaller or similar increases in globally, annually averaged N80 attributable to sub-grid sulphate than two other previously used assumptions for sub-grid sulphate, depending on model assumptions regarding SOA and nucleation. When using previous treatments of sub-grid sulphate, including an additional $100 \, \text{Tg yr}^{-1}$ of SOA led to an increase in the N80 attributable to sub-grid sulphate particles. This increase was due to an enhancement in condensational growth of the sub-grid sulphate particles. The proportion of global N80 attributable to sub-grid sulphate depends not only on the choice of sub-grid sulphate scheme, but also on other model parameters and processes that affect pre-existing N80 and the grid-resolved condensational growth of sub-grid sulphate.

However, the number of new sub-grid sulphate particles predicted by the P6 parameterization depends strongly on the pre-existing aerosol condensation sink. The additional SOA increased the pre-existing condensation sink, drastically decreasing the sub-grid new-particle formation predicted by the P6 parameterization, and decreasing the influence of sub-grid sulphate on N80. For sufficiently large pre-existing condensation sink, the P6 sub-grid sulphate scheme predicted that nearly all sub-grid sulphate would condense onto pre-existing particles, and the growth of these particles resulted in enhanced coagulational losses and more efficient removal by deposition, producing little change in aerosol number concentrations.

In addition, we tested the sensitivity of the results of GEOS-Chem-TOMAS with P6 sub-grid sulphate to changes in emissions. We found that for a global increase in emissions of 50 %, globally, annually averaged N80 increased by 9.00 % (SO_2), 1.47 % (NO_x), or 10.24 % (SO_2 and NO_x). Both the size and number of sub-grid sulphate particles emitted increased with increasing SO_2 emissions, as did the grid-resolved concentrations of SO_2 available to form SO_4. Both sub-grid and grid-resolved oxidation of SO_2 increase with increasing NO_x emissions, except in very polluted regions ([NO_x]>1 ppb), where oxidation rates increase with decreasing NO_x concentrations. Both the number and size of sub-grid particles decrease with increasing NO_x emissions. When both SO_2 and NO_x emissions increase, the number of sub-grid sulphate particles emitted decreases over polluted regions and increases over remote regions, and there is little change in the size of sub-grid sulphate particles.

Finally, we have compared the simulated annually averaged N10, N40, N80, and N150 against those measured at 21 surface-based measurement sites. Differences in sub-grid sulphate scheme were not found to strongly affect the number concentrations in these size ranges at these sites. For cases without anthropogenically controlled SOA, the absolute log-mean bias between simulated and observed number concentrations was reduced by including any sub-grid sulphate scheme. When anthropogenically controlled SOA was included, the AS3 and LY5 schemes tended to increase the absolute log-mean bias. The P6 sub-grid sulphate scheme only slightly altered the absolute log-mean bias from the case with no sub-grid sulphate. This was due to the reduction in new-particle formation predicted under higher condensation sink conditions. The R^2 values for N80 and N150 were highest when using the P6 sub-grid sulphate scheme, regardless of SOA amount or grid-resolved nucleation scheme. For the Activation-type grid-resolved nucleation cases, the P6 sub-grid sulphate scheme also yielded the highest R^2 values for the N10 and N40. We believe that the P6 scheme yields better correlation with observations because the differences in sub-grid scale new-particle formation and growth under different conditions predicted by the P6 sub-grid sulphate scheme allows it to better represent spatial heterogeneity in these processes than constant assumptions about the number and size of sulphate formed at the sub-grid scale.

The additional anthropogenically controlled SOA included in many of our simulations would be expected to condense onto the newly formed particles at the sub-grid scale, a process that is not currently resolved by P6. Anthropogenically controlled SOA may preferentially form in coal-fired power-plant plumes, and so this additional SOA may condense preferentially onto particles formed within these plumes compared to pre-existing particles. The P6 parameterization therefore likely underestimates the number and size of newly formed particles in simulations where anthropogenically controlled SOA is included. However, we note that when the anthropogenically controlled SOA was included, the simulations with P6 sub-grid sulphate had smaller absolute log-mean biases from observed aerosol number concentrations than the simulations with AS3 or LY5 sub-grid sulphate, and similar absolute log-mean biases to the simulations with no sub-grid sulphate. This would suggest that the number of newly formed particles predicted by P6 when anthropogenically controlled SOA is included may be more realistic than the number of newly formed particles predicted by the AS3 or LY5 sub-grid sulphate assumptions. Other uncertain model processes also influence aerosol number concentrations, so it is also possible that the P6 parameterization benefits from a cancelling of errors in this case. We intend to include sub-grid condensation of SOA in a future version of P6 to better resolve these uncertainties.

Due to the physical basis of the P6 parameterization, we believe it to yield more representative predictions for the number and size of aerosol formed than previous assumptions about sub-grid sulphate. Moreover, no constant assumption about the number and size of sub-grid sulphate formed can resolve differences in new-particle formation and growth due to changes in background chemical or meteorological conditions. However, the differences between simulated size distributions at the surface-based measurement sites considered in this work were too small to establish P6 as unambiguously providing better agreement with observations. Continuing evaluation of the P6 parameterization against observations is therefore planned as future work.

Edited by: V.-M. Kerminen

References

Aalto, P., Hämeri, K., Becker, E., Weber, R., Salm, J., Mäkelä, J. M., Hoell, C., O'Dowd, C. D., Karlsson, H., Hansson, H.-C., Väkevä, M., Koponen, I. K., Buzorius, G., and Kulmala, M.: Physical characterization of aerosol particles during nucleation events, Tellus B, 53, 344–358, 2001.

Adams, P. J. and Seinfeld, J. H.: Predicting global aerosol size distributions in general circulation models, J. Geophys. Res., 107, 1–23, 2002.

Adams, P. J. and Seinfeld, J. H.: Disproportionate impact of particulate emissions on global cloud condensation nuclei concentrations, Geophys. Res. Lett., 30, 1239, 2003.

Albrecht, B.: Aerosols, cloud microphysics, and fractional cloudiness., Science, 245, 1227–1230, 1989.

Arya, S. P.: Air Pollution Meteorology and Dispersion, Oxford University Press, Inc., New York, USA, 1999.

Asmi, A., Wiedensohler, A., Laj, P., Fjaeraa, A.-M., Sellegri, K., Birmili, W., Weingartner, E., Baltensperger, U., Zdimal, V., Zikova, N., Putaud, J.-P., Marinoni, A., Tunved, P., Hansson, H.-C., Fiebig, M., Kivekäs, N., Lihavainen, H., Asmi, E., Ulevicius, V., Aalto, P. P., Swietlicki, E., Kristensson, A., Mihalopoulos, N., Kalivitis, N., Kalapov, I., Kiss, G., de Leeuw, G., Henzing, B., Harrison, R. M., Beddows, D., O'Dowd, C., Jennings, S. G., Flentje, H., Weinhold, K., Meinhardt, F., Ries, L., and Kulmala, M.: Number size distributions and seasonality of submicron particles in Europe 2008–2009, Atmos. Chem. Phys., 11, 5505–5538, doi:10.5194/acp-11-5505-2011, 2011.

Auvray, M. and Bey, I.: Long-range transport to Europe: Seasonal variations and implications for the European ozone budget, J. Geophys. Res., 110, D11303, 2005.

Bey, I., Jacob, D. J., Yantosca, R. M., Logan, J. a., Field, B. D., Fiore, A. M., Li, Q., Liu, H. Y., Mickley, L. J., and Schultz, M. G.: Global modeling of tropospheric chemistry with assimilated meteorology: Model description and evaluation, J. Geophys. Res., 106, 23073, 2001.

Boucher, O., Randall, D., Artaxo, P., Bretherton, C., Feingold, G., Forster, P., Kerminen, V.-M., Kondo, Y., Liao, H., Lohmann, U., Rasch, P., Satheesh, S., Sherwood, S., Stevens, B., and Zhang, X.: Clouds and Aerosols, in: Climate Change 2013: The Physical Science Basis. Contribution of Working Group I to the Fifth Assessment Report of the Intergovernmental Panel on Climate Change, edited by Stocker, T., Qin, D., Plattner, G.-K., Tignor, M., Allen, S., Boschung, J., Nauels, A., Xia, Y., Bex, V., and Midgley, P., chap. 7, pp. 571–657, Cambridge University Press, Cambridge, UK and New York, NY, USA, 2013.

Carlton, A. G., Wiedinmyer, C., and Kroll, J. H.: A review of Secondary Organic Aerosol (SOA) formation from isoprene, Atmos. Chem. Phys., 9, 4987–5005, doi:10.5194/acp-9-4987-2009, 2009.

Carlton, A. G., Pinder, R. W., Bhave, P. V., and Pouliot, G. A.: To what extent can biogenic SOA be controlled?, Environ. Sci. Technol., 44, 3376–80, 2010.

Charlson, R. J., Schwartz, S. E., Hales, J. M., Cess, R. D., Coakley, J. a., Hansen, J. E., and Hofmann, D. J.: Climate forcing by anthropogenic aerosols., Science, 255, 423–430, 1992.

D'Andrea, S. D., Häkkinen, S. A. K., Westervelt, D. M., Kuang, C., Levin, E. J. T., Kanawade, V. P., Leaitch, W. R., Spracklen, D. V., Riipinen, I., and Pierce, J. R.: Understanding global secondary organic aerosol amount and size-resolved condensational behav-

ior, Atmos. Chem. Phys., 13, 11519–11534, doi:10.5194/acp-13-11519-2013, 2013.

Dentener, F., Kinne, S., Bond, T., Boucher, O., Cofala, J., Generoso, S., Ginoux, P., Gong, S., Hoelzemann, J. J., Ito, A., Marelli, L., Penner, J. E., Putaud, J.-P., Textor, C., Schulz, M., van der Werf, G. R., and Wilson, J.: Emissions of primary aerosol and precursor gases in the years 2000 and 1750 prescribed data-sets for AeroCom, Atmos. Chem. Phys., 6, 4321–4344, doi:10.5194/acp-6-4321-2006, 2006.

Dockery, D., Pope, C., Xu, X., Spengler, J. D., Ware, J. H., Fay, M. E., Ferris, B. G., and Speizer, F. E.: An association between air pollution and mortality in six US cities, New Engl. J. Med., 329, 1753–1759, 1993.

Dusek, U., Frank, G. P., Hildebrandt, L., Curtius, J., Schneider, J., Walter, S., Chand, D., Drewnick, F., Hings, S., Jung, D., Borrmann, S., and Andreae, M. O.: Size matters more than chemistry for cloud-nucleating ability of aerosol particles., Science, 312, 1375–8, 2006.

Eisele, F. and Tanner, D.: Measurement of the gas phase concentration of H2SO4 and methane sulfonic acid and estimates of H2SO4 production and loss in the atmosphere, J. Geophys. Res., 98, 9001–9010, 1993.

Erupe, M. E., Benson, D. R., Li, J., Young, L.-H., Verheggen, B., Al-Refai, M., Tahboub, O., Cunningham, V., Frimpong, F., Viggiano, A. a., and Lee, S.-H.: Correlation of aerosol nucleation rate with sulfuric acid and ammonia in Kent, Ohio: An atmospheric observation, J. Geophys. Res., 115, D23216, 2010.

Guenther, A., Karl, T., Harley, P., Wiedinmyer, C., Palmer, P. I., and Geron, C.: Estimates of global terrestrial isoprene emissions using MEGAN (Model of Emissions of Gases and Aerosols from Nature), Atmos. Chem. Phys., 6, 3181–3210, doi:10.5194/acp-6-3181-2006, 2006.

Heald, C. L., Coe, H., Jimenez, J. L., Weber, R. J., Bahreini, R., Middlebrook, A. M., Russell, L. M., Jolleys, M., Fu, T.-M., Allan, J. D., Bower, K. N., Capes, G., Crosier, J., Morgan, W. T., Robinson, N. H., Williams, P. I., Cubison, M. J., DeCarlo, P. F., and Dunlea, E. J.: Exploring the vertical profile of atmospheric organic aerosol: comparing 17 aircraft field campaigns with a global model, Atmos. Chem. Phys., 11, 12673–12696, doi:10.5194/acp-11-12673-2011, 2011.

Heald, C. L., Collett Jr., J. L., Lee, T., Benedict, K. B., Schwandner, F. M., Li, Y., Clarisse, L., Hurtmans, D. R., Van Damme, M., Clerbaux, C., Coheur, P.-F., Philip, S., Martin, R. V., and Pye, H. O. T.: Atmospheric ammonia and particulate inorganic nitrogen over the United States, Atmos. Chem. Phys., 12, 10295–10312, doi:10.5194/acp-12-10295-2012, 2012.

Jung, J., Fountoukis, C., Adams, P. J., and Pandis, S. N.: Simulation of in situ ultrafine particle formation in the eastern United States using PMCAMx-UF, J. Geophys. Res. Atmos., 115, doi:10.1029/2009JD012313, 2010.

Junkermann, W., Vogel, B., and Sutton, M. A.: The climate penalty for clean fossil fuel combustion, Atmos. Chem. Phys., 11, 12917–12924, doi:10.5194/acp-11-12917-2011, 2011.

Kanawade, V. P., Benson, D. R., and Lee, S.-H.: Statistical analysis of 4-year observations of aerosol sizes in a semi-rural continental environment, Atmos. Environ., 59, 30–38, 2012.

Kerminen, V.-M., and Kulmala, M.: Analytical formulae connecting the "real" and the "apparent" nucleation rate and the nuclei num-

ber concentration for atmospheric nucleation events, J. Aerosol Sci., 33, 609–622, doi:10.1016/S0021-8502(01)00194-X, 2002.

Khairoutdinov, M. and Randall, D.: Cloud resolving modeling of the ARM summer 1997 IOP: Model formulation, results, uncertainties, and sensitivities, J. Atmos. Sci., 60, 607–626, 2003.

Kuhns, H., Green, M., and Etyemezian, V.: Big Bend Regional Aerosol and Visibility Observational (BRAVO) Study Emissions Inventory, technical report prepared for the BRAVO Steering Committee, Tech. Rep. 702, 2001.

Kulmala, M. and Kerminen, V.-M.: On the formation and growth of atmospheric nanoparticles, Atmos. Res., 90, 132–150, 2008.

Kulmala, M., Lehtinen, K. E. J., and Laaksonen, A.: Cluster activation theory as an explanation of the linear dependence between formation rate of 3nm particles and sulphuric acid concentration, Atmos. Chem. Phys., 6, 787–793, doi:10.5194/acp-6-787-2006, 2006.

Leaitch, W. R., Sharma, S., Huang, L., Toom-Sauntry, D., Chivulescu, A., Macdonald, A. M., von Salzen, K., Pierce, J. R., Bertram, A. K., Schroder, J. C., Shantz, N. C., Chang, R. Y.-W., and Norman, A.-L.: Dimethyl sulfide control of the clean summertime Arctic aerosol and cloud, Elementa: Science of the Anthropocene, 1, 000017, 2013.

Lee, L. A., Pringle, K. J., Reddington, C. L., Mann, G. W., Stier, P., Spracklen, D. V., Pierce, J. R., and Carslaw, K. S.: The magnitude and causes of uncertainty in global model simulations of cloud condensation nuclei, Atmos. Chem. Phys., 13, 8879–8914, doi:10.5194/acp-13-8879-2013, 2013.

Lee, Y. H. and Adams, P. J.: A Fast and Efficient Version of the TwO-Moment Aerosol Sectional (TOMAS) Global Aerosol Microphysics Model, Aerosol Sci. Tech., 46, 678–689, 2012.

Levin, E., Kreidenweis, S., McMeeking, G., Carrico, C., Collett Jr., J., and Malm, W.: Aerosol physical, chemical and optical properties during the Rocky Mountain Airborne Nitrogen and Sulfur study, Atmos. Environ., 43, 1932–1939, 2009.

Levin, E. J. T., Prenni, a. J., Petters, M. D., Kreidenweis, S. M., Sullivan, R. C., Atwood, S. a., Ortega, J., DeMott, P. J., and Smith, J. N.: An annual cycle of size-resolved aerosol hygroscopicity at a forested site in Colorado, J. Geophys. Res., 117, D06201, 2012.

Lonsdale, C. R., Stevens, R. G., Brock, C. A., Makar, P. A., Knipping, E. M., and Pierce, J. R.: The effect of coal-fired power-plant SO_2 and NO_x control technologies on aerosol nucleation in the source plumes, Atmos. Chem. Phys., 12, 11519–11531, doi:10.5194/acp-12-11519-2012, 2012.

Luo, G. and Yu, F.: Sensitivity of global cloud condensation nuclei concentrations to primary sulfate emission parameterizations, Atmos. Chem. Phys., 11, 1949–1959, doi:10.5194/acp-11-1949-2011, 2011.

Makkonen, R., Asmi, A., Korhonen, H., Kokkola, H., Järvenoja, S., Räisänen, P., Lehtinen, K. E. J., Laaksonen, A., Kerminen, V.-M., Järvinen, H., Lohmann, U., Bennartz, R., Feichter, J., and Kulmala, M.: Sensitivity of aerosol concentrations and cloud properties to nucleation and secondary organic distribution in ECHAM5-HAM global circulation model, Atmos. Chem. Phys., 9, 1747–1766, doi:10.5194/acp-9-1747-2009, 2009.

Mesinger, F., DiMego, G., Kalnay, E., Mitchell, K., Shafran, P. C., Ebisuzaki, W., Jović, D., Woollen, J., Rogers, E., Berbery, E. H., Ek, M. B., Fan, Y., Grumbine, R., Higgins, W., Li, H., Lin, Y., Manikin, G., Parrish, D., and Shi, W.: North American Regional Reanalysis, B. Am. Meteorol. Soc., 87, 343–360, 2006.

Napari, I., Noppel, M., Vehkamäki, H., and Kulmala, M.: Parametrization of ternary nucleation rates for H_2SO_4-NH_3-H_2O vapors, J. Geophys. Res., 107, 4381, 2002.

Offenberg, J. H., Lewandowski, M., Edney, E. O., Kleindienst, T. E., and Jaoui, M.: Influence of aerosol acidity on the formation of secondary organic aerosol from biogenic precursor hydrocarbons., Environ. Sci. Technol., 43, 7742–7, 2009.

Olivier, J. G. J., Bouwman, A. F., Van der Maas, C. W. M., Berdowski, J. J. M., Veldt, C., Bloos, J. P. J., Visschedijk, A. J. H., Zandveld, P. Y. J., and Haverlag, J. L.: RIVM report nr. 771060002 / TNO-MEP report nr. R96/119: Description of EDGAR Version 2.0: A set of global emission inventories of greenhouse gases and ozone-depleting substances for all anthropogenic and most natural sources on a per country basis and on $1° \times 1°$ grid., Tech. rep., Netherlands Organization for Applied Scientific Research (TNO), 1996.

Olson, J. R., Crawford, J. H., Chen, G., Brune, W. H., Faloona, I. C., Tan, D., Harder, H., and Martinez, M.: A reevaluation of airborne HO_x observations from NASA field campaigns, J. Geophys. Res., 111, D10301, 2006.

Peng, R. D., Dominici, F., Pastor-Barriuso, R., Zeger, S. L., and Samet, J. M.: Seasonal analyses of air pollution and mortality in 100 US cities., Am. J. Epidemiol., 161, 585–94, 2005.

Peters, A., Wichmann, H. E., Tuch, T., Heinrich, J., and Heyder, J.: Respiratory effects are associated with the number of ultrafine particles., Am. J. Resp. Crit. Care, 155, 1376–1383, 1997.

Pierce, J. R. and Adams, P. J.: Global evaluation of CCN formation by direct emission of sea salt and growth of ultrafine sea salt, J. Geophys. Res., 111, D06203, 2006.

Pierce, J. R. and Adams, P. J.: Uncertainty in global CCN concentrations from uncertain aerosol nucleation and primary emission rates, Atmos. Chem. Phys., 9, 1339–1356, doi:10.5194/acp-9-1339-2009, 2009.

Pierce, J. R., Chen, K., and Adams, P. J.: Contribution of primary carbonaceous aerosol to cloud condensation nuclei: processes and uncertainties evaluated with a global aerosol microphysics model, Atmos. Chem. Phys., 7, 5447–5466, doi:10.5194/acp-7-5447-2007, 2007.

Pierce, J. R., Leaitch, W. R., Liggio, J., Westervelt, D. M., Wainwright, C. D., Abbatt, J. P. D., Ahlm, L., Al-Basheer, W., Cziczo, D. J., Hayden, K. L., Lee, A. K. Y., Li, S.-M., Russell, L. M., Sjostedt, S. J., Strawbridge, K. B., Travis, M., Vlasenko, A., Wentzell, J. J. B., Wiebe, H. A., Wong, J. P. S., and Macdonald, A. M.: Nucleation and condensational growth to CCN sizes during a sustained pristine biogenic SOA event in a forested mountain valley, Atmos. Chem. Phys., 12, 3147–3163, doi:10.5194/acp-12-3147-2012, 2012.

Pierce, J. R., Evans, M. J., Scott, C. E., D'Andrea, S. D., Farmer, D. K., Swietlicki, E., and Spracklen, D. V.: Weak global sensitivity of cloud condensation nuclei and the aerosol indirect effect to Criegee + SO_2 chemistry, Atmos. Chem. Phys., 13, 3163–3176, doi:10.5194/acp-13-3163-2013, 2013.

Reddington, C. L., Carslaw, K. S., Spracklen, D. V., Frontoso, M. G., Collins, L., Merikanto, J., Minikin, A., Hamburger, T., Coe, H., Kulmala, M., Aalto, P., Flentje, H., Plass-Dülmer, C., Birmili, W., Wiedensohler, A., Wehner, B., Tuch, T., Sonntag, A., O'Dowd, C. D., Jennings, S. G., Dupuy, R., Baltensperger, U., Weingartner, E., Hansson, H.-C., Tunved, P., Laj, P., Sellegri, K., Boulon, J., Putaud, J.-P., Gruening, C., Swi-

etlicki, E., Roldin, P., Henzing, J. S., Moerman, M., Mihalopoulos, N., Kouvarakis, G., Žďímal, V., Zíková, N., Marinoni, A., Bonasoni, P., and Duchi, R.: Primary versus secondary contributions to particle number concentrations in the European boundary layer, Atmos. Chem. Phys., 11, 12007–12036, doi:10.5194/acp-11-12007-2011, 2011.

Rienecker, M.: File Specification for GEOS-5 DAS Gridded Output, Tech. rep., Global Modeling and Assimilation Office, Goddard Space Flight Center, Greenbelt, Maryland, 2006.

Riipinen, I., Pierce, J. R., Yli-Juuti, T., Nieminen, T., Häkkinen, S., Ehn, M., Junninen, H., Lehtipalo, K., Petäjä, T., Slowik, J., Chang, R., Shantz, N. C., Abbatt, J., Leaitch, W. R., Kerminen, V.-M., Worsnop, D. R., Pandis, S. N., Donahue, N. M., and Kulmala, M.: Organic condensation: a vital link connecting aerosol formation to cloud condensation nuclei (CCN) concentrations, Atmos. Chem. Phys., 11, 3865–3878, doi:10.5194/acp-11-3865-2011, 2011.

Sihto, S.-L., Kulmala, M., Kerminen, V.-M., Dal Maso, M., Petäjä, T., Riipinen, I., Korhonen, H., Arnold, F., Janson, R., Boy, M., Laaksonen, A., and Lehtinen, K. E. J.: Atmospheric sulphuric acid and aerosol formation: implications from atmospheric measurements for nucleation and early growth mechanisms, Atmos. Chem. Phys., 6, 4079–4091, doi:10.5194/acp-6-4079-2006, 2006.

Snow-Kropla, E. J., Pierce, J. R., Westervelt, D. M., and Trivitayanurak, W.: Cosmic rays, aerosol formation and cloud-condensation nuclei: sensitivities to model uncertainties, Atmos. Chem. Phys., 11, 4001–4013, doi:10.5194/acp-11-4001-2011, 2011.

Spracklen, D. V., Pringle, K. J., Carslaw, K. S., Chipperfield, M. P., and Mann, G. W.: A global off-line model of size-resolved aerosol microphysics: II. Identification of key uncertainties, Atmos. Chem. Phys., 5, 3233–3250, doi:10.5194/acp-5-3233-2005, 2005.

Spracklen, D. V., Jimenez, J. L., Carslaw, K. S., Worsnop, D. R., Evans, M. J., Mann, G. W., Zhang, Q., Canagaratna, M. R., Allan, J., Coe, H., McFiggans, G., Rap, A., and Forster, P.: Aerosol mass spectrometer constraint on the global secondary organic aerosol budget, Atmos. Chem. Phys., 11, 12109–12136, doi:10.5194/acp-11-12109-2011, 2011.

Srivastava, R. K., Miller, C. a., Erickson, C., and Jambhekar, R.: Emissions of sulfur trioxide from coal-fired power plants., J. Air Waste Manage., 54, 750–62, 2004.

Stevens, R. G. and Pierce, J. R.: A parameterization of sub-grid particle formation in sulfur-rich plumes for global- and regional-scale models, Atmos. Chem. Phys., 13, 12117–12133, doi:10.5194/acp-13-12117-2013, 2013.

Stevens, R. G., Pierce, J. R., Brock, C. A., Reed, M. K., Crawford, J. H., Holloway, J. S., Ryerson, T. B., Huey, L. G., and Nowak, J. B.: Nucleation and growth of sulfate aerosol in coal-fired power plant plumes: sensitivity to background aerosol and meteorology, Atmos. Chem. Phys., 12, 189–206, doi:10.5194/acp-12-189-2012, 2012.

Stieb, D. M., Judek, S., and Burnett, R. T.: Meta-analysis of time-series studies of air pollution and mortality: effects of gases and particles and the influence of cause of death, age, and season., J. Air Waste Manage., 52, 470–484, 2002.

Streets, D. G., Bond, T. C., Carmichael, G. R., Fernandes, S. D., Fu, Q., He, D., Klimont, Z., Nelson, S. M., Tsai, N. Y., Wang, M. Q., Woo, J.-H., and Yarber, K. F.: An inventory of gaseous and primary aerosol emissions in Asia in the year 2000, J. Geophys. Res., 108, 8809, 2003.

Surratt, J. D., Lewandowski, M., Offenberg, J. H., Jaoui, M., Kleindienst, T. E., Edney, E. O., and Seinfeld, J. H.: Effect of acidity on secondary organic aerosol formation from isoprene., Environ. Sci. Technol., 41, 5363–9, 2007.

Trivitayanurak, W., Adams, P. J., Spracklen, D. V., and Carslaw, K. S.: Tropospheric aerosol microphysics simulation with assimilated meteorology: model description and intermodel comparison, Atmos. Chem. Phys., 8, 3149–3168, doi:10.5194/acp-8-3149-2008, 2008.

Twomey, S.: Pollution and planetary albedo, Atmos. Environ., 8, 1251–1256, 1974.

United States Environmental Protection Agency: Clean Air Markets: Data and Maps, http://ampd.epa.gov/ampd/ (last access: March 2013), 2012.

van der Werf, G. R., Randerson, J. T., Giglio, L., Collatz, G. J., Mu, M., Kasibhatla, P. S., Morton, D. C., DeFries, R. S., Jin, Y., and van Leeuwen, T. T.: Global fire emissions and the contribution of deforestation, savanna, forest, agricultural, and peat fires (1997–2009), Atmos. Chem. Phys., 10, 11707–11735, doi:10.5194/acp-10-11707-2010, 2010.

Vehkamäki, H., Kulmala, M., Napari, I., Lehtinen, K. E. J., Timmreck, C., Noppel, M., and Laaksonen, A.: An improved parameterization for sulfuric acid–water nucleation rates for tropospheric and stratospheric conditions, J. Geophys. Res., 107, 4622, 2002.

Walker, J. M., Philip, S., Martin, R. V., and Seinfeld, J. H.: Simulation of nitrate, sulfate, and ammonium aerosols over the United States, Atmos. Chem. Phys., 12, 11213–11227, doi:10.5194/acp-12-11213-2012, 2012.

Wang, M. and Penner, J. E.: Aerosol indirect forcing in a global model with particle nucleation, Atmos. Chem. Phys., 9, 239–260, doi:10.5194/acp-9-239-2009, 2009.

Wang, S. C. and Flagan, R. C.: Scanning Electrical Mobility Spectrometer, Aerosol Sci. Tech., 13, 230–240, 1990.

Westervelt, D. M., Pierce, J. R., Riipinen, I., Trivitayanurak, W., Hamed, A., Kulmala, M., Laaksonen, A., Decesari, S., and Adams, P. J.: Formation and growth of nucleated particles into cloud condensation nuclei: model–measurement comparison, Atmos. Chem. Phys., 13, 7645–7663, doi:10.5194/acp-13-7645-2013, 2013.

Westervelt, D. M., Pierce, J. R., and Adams, P. J.: Analysis of feedbacks between nucleation rate, survival probability and cloud condensation nuclei formation, Atmos. Chem. Phys., 14, 5577–5597, doi:10.5194/acp-14-5577-2014, 2014.

Yu, F. and Luo, G.: Simulation of particle size distribution with a global aerosol model: contribution of nucleation to aerosol and CCN number concentrations, Atmos. Chem. Phys., 9, 7691–7710, doi:10.5194/acp-9-7691-2009, 2009.